Electroweak physics at the LHC

J Berryhill[1] and A Oh[2]

[1] Fermi National Accelerator Laboratory, Batavia, IL, USA

[2] School of Physics and Astronomy, University of Manchester, Manchester, UK

Abstract. The Large Hadron Collider (LHC) has completed in 2012 its first running phase and the experiments have collected data sets of pp collisions at center-of-mass energies of 7 and 8 TeV with an integrated luminosity of about 5 $\text{fb}^{-1}$and 20 fb^{-1}, respectively. Analyses of these data sets have produced a rich set of results in the electroweak sector of the standard model. This article reviews the status of electroweak measurements of the ATLAS and CMS experiments at the LHC and discusses phenomenological developments in the electroweak sector.

PACS numbers: 12.15.-y, 12.60.Cn, 14.70.-e

Submitted to: *J. Phys. G: Nucl. Part. Phys.*

1. Introduction

With the discovery of the Higgs boson in 2012 [1, 2] the standard model of particle physics seemed complete, but fundamental questions remain to be answered, as for example about the constituents of dark matter, the relative abundance of matter over anti-matter, and the unification of forces at the Planck scale.

The standard model of the electroweak interactions is a quantum field theory unifying the electromagnetic and the weak force into one gauge theory transforming under the gauge group $SU_L(2) \otimes U_{EM}(1)$. The electro-weak Lagrangian can be represented as

$$\mathcal{L}_{EW} = \mathcal{L}_{boson} + \mathcal{L}_{fermion} + \mathcal{L}_{higgs} + \mathcal{L}_{yukawa}$$

with $\mathcal{L}_{boson}$ the kinetic and self-interaction term of bosons, $\mathcal{L}_{fermion}$ the kinetic term describing the interacion of fermions with bosons, $\mathcal{L}_{higgs}$ the Higgs term which generates the gauge boson masses and coupling to the Higgs field, and the Yukawa term $\mathcal{L}_{yukawa}$ describing the interaction between the fermion and Higgs field. Precision measurements in the electro-weak sector allow to test the plausibility of various extensions to the standard model Lagrangian. In the framework of anomalous gauge couplings and it's reformulation as effective field theory, the standard model can be extended with additional generic terms in the Lagrangian to describe new physics. The measurement of electroweak production processes allows to verify the validity of the standard model in this framework at the high collision energies the Large Hadron Collider (LHC) is providing.

The LHC was designed to primarily search for the Higgs boson and new phenomena, but the requirements of proton-proton collisions at high collision energy and luminosity also enable precision electroweak measurements. The LHC provides a rich testing ground to benchmark perturbative QCD over a wide range of scales, and to determine the structure of the proton. Both are essential ingredients to make precise electroweak measurements, as higher order corrections in perturbative QCD have a substantial effect on the theoretical predictions to standard model processes, and the knowledge of the proton structure becomes a major uncertainty for processes with very high partonic centre of mass, i.e. the region where new physics is expected to become visible.

The LHC collides protons on protons in a circular ring of 27 km circumference with an energy of up to 7 TeV per beam, corresponding to a collision energy at the centre-of-mass of $\sqrt{s} = 14$ TeV, and a design luminosity of 10^{34} cm^{-2} s^{-1}. The two general purpose detectors at the LHC, ATLAS and CMS, are able to record a wide range of physics process. They differ in the technical details of detector layout and data-acquisition design but have common design goals, namely good detector coverage for charged and neutral particles, excellent resolution to measure the positions and momenta of charged particles, and precision calorimetry. The other two main experiments at the LHC are optimized for recording collision of heavy ions in the case of ALICE or for precision measurements of b-hadrons and CP violation (LHC-b).

In the run period from 2010 to 2011 about 6 fb^{-1} of integrated luminosity at a centre-of-mass energy $\sqrt{s} = 7$ TeV were delivered. In 2012 the energy was raised to $\sqrt{s} = 8$ TeV and the integrated luminosity produced was 23 fb^{-1}. After a long shutdown LHC resumed running in 2015 at an increased energy of $\sqrt{s} = 13$ TeV, and was able to provide 4.5 fb^{-1} of collision data. The experiments ATLAS and CMS have published results on all three data sets, but the majority of electroweak results available up to now are based mainly on the full 7 TeV and partly on the full 8 TeV data sets. Generally, the precision measurements of cross section and differential distributions involve more analysis effort compared to e.g. searches for new resonances, hence the different time-scale for this category of measurements.

In the following we will give brief review of recent theory developments (section 2), and a comprehensive summary of the electroweak results from ATLAS and CMS. In section **??** we summarise the results on inclusive vector boson production (Drell-Yan process, inclusive di-boson and tri-boson production), and continue in section **??** with exclusive boson production in the vector boson fusion and vector boson scattering processes. Finally, the LHC results on electroweak precision tests are discussed in section **??**.

2. Theory overview and recent developments

2.1. PDF and electroweak observables (V+jets, ϕ^*)

2.2. Electroweak NLO corrections

2.3. Anomalous gauge couplings and effective field theory

2.4. Oblique corrections, constructed observables

3. Inclusive boson production

3.1. Drell-Yan production

At a hadron collider, the most fundamental tests of electroweak boson couplings to fermions are measurements of the kinematic properties of Drell-Yan (DY) lepton pair production. At leading order, Drell-Yan production occurs when a quark–anti-quark pair in the intial state annihilates into an electroweak boson, which subsequently decays to a lepton pair. Differential cross section calculations exist for next-to-next-to leading order (NNLO) QCD corrections as well as NLO electroweak corrections. In the EFT context, such a process is sensitive to four-fermion contact interactions of the type

$$\begin{aligned}\mathcal{L} = \tfrac{g^2}{\Lambda^2} \big[\quad & \eta_{\text{LL}} \, (\overline{q}_{\text{L}}\gamma_\mu q_{\text{L}}) \, (\overline{\ell}_{\text{L}}\gamma^\mu \ell_{\text{L}}) \\ & + \eta_{\text{RR}} \, (\overline{q}_{\text{R}}\gamma_\mu q_{\text{R}}) \, (\overline{\ell}_{\text{R}}\gamma^\mu \ell_{\text{R}}) \\ & + \eta_{\text{LR}} \, (\overline{q}_{\text{L}}\gamma_\mu q_{\text{L}}) \, (\overline{\ell}_{\text{R}}\gamma^\mu \ell_{\text{R}}) \\ & + \eta_{\text{RL}} \, (\overline{q}_{\text{R}}\gamma_\mu q_{\text{R}}) \, (\overline{\ell}_{\text{L}}\gamma^\mu \ell_{\text{L}}) \big] ,\end{aligned} \tag{1}$$

where g is a coupling constant, Λ is the contact interaction scale, and $q_{\mathrm{L,R}}$ and $\ell_{\mathrm{L,R}}$ are left-handed and right-handed quark and lepton fields, respectively. The parameters $\eta_{i,j}$ denote the relative interference of the operators; the experiments have considered the cases $\eta_{\mathrm{LR}} = \eta_{\mathrm{RL}} = \pm 1$, $\eta_{\mathrm{LL}} = \pm 1$, or $\eta_{\mathrm{RR}} = \pm 1$.

Experiments select electron or muon pairs above trigger thresholds: CMS selects leading lepton $p_T > 17$ GeV and second leading lepton $p_T > 8$ GeV inclusively, and ATLAS selects high mass events with both lepton $p_T > 25$ GeV. Backgrounds to Drell-Yan production are relatively small, and consist of real prompt lepton pair production from top quark or boson pairs, as well as fake electrons from QCD jets. The real lepton pair background is flavor democratic, and can therefore be reliably estimated from $e\mu$ pair production. Fake electron production is typically estimated from background enriched QCD jet samples, from which the fake electron rate can be measured, convolved with electron-jet control samples.

Figure 1 shows the Drell-Yan cross section at high electron pair mass measured by ATLAS at 7 TeV [3]. The cross section uncertainty is predominantly systematic below 400 GeV in pair mass and predominantly statistical above 400 GeV. The data are compared with an NNLO QCD prediction with NLO electroweak corrections, provided by the FEWZ 3.1 generator [4, 5]. The prediction also includes photon induced lepton pair production, which generally increases cross section estimates by a few percent. The FEWZ prediction generally underestimates the cross section, however a correlated chi-squared analysis concludes that this is not statistically significant.

Figure 2 shows the Drell-Yan cross section for electron or muon pairs measured by CMS at 8 TeV [6]. Agreement with the FEWZ prediction is observed over the entire measured mass range, from 15 GeV to 2000 GeV. CMS has also measured the double differential cross section with respect to dilepton rapidity in several bins of dilepton mass, as well as a differential cross section ratio between the 8 TeV and 7 TeV data, which has small experimental and theoretical uncertainties.

In the absence of observed disagreements with predictions at the highest dilepton masses, the data are analyzed to constrain the size of anomalous contact interactions. Assuming a fixed, strong value for the coupling ($g^2/4\pi = 1$), limits can be obtained on the contact interaction scale Λ. ATLAS estimates a lower limit of 17 to 26 TeV on Λ, where the strongest lower limits correspond to constructive interference scenarios (especially LR+RL), and the weakest to destructive interference scenarios [7]. CMS has limits with similar sensitivity estimated for LL contact interactions [8].

3.2. Inclusive di-boson production

3.2.1. ZZ production The production of ZZ in proton-proton collisions has been one of the first di-boson processes measured at the LHC. The SM process is and an important and irreducible background to resonance searches and Higgs production. The production at leading order is dominated by quark anti-quark annihilation in the t and u-channel, whereas the s-channel process is forbidden in the SM (see also Figure 3). The gluon

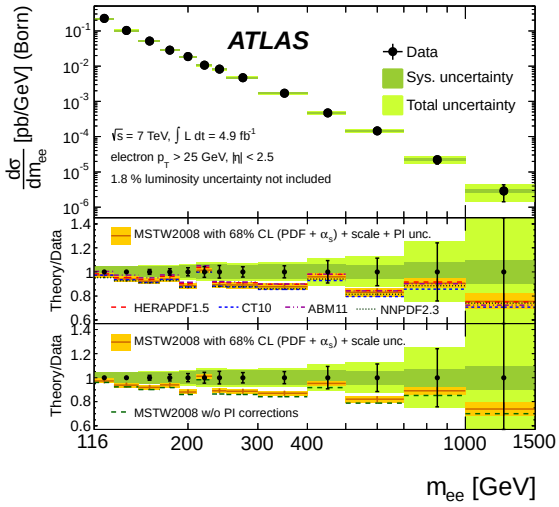

Figure 1. Measured differential cross-section at the Born level within the fiducial region (electron $p_{\mathrm{T}} > 25$ GeV and $|\eta| < 2.5$) with statistical, systematic, and combined statistical and systematic (total) uncertainties, excluding the 1.8% uncertainty on the luminosity. On the left, in the upper ratio plot, the photon-induced (PI) corrections have been added to the predictions obtained from the MSTW2008, HERAPDF1.5, CT10, ABM11 and NNPDF2.3 NNLO PDFs, and for the MSTW2008 prediction the total uncertainty band arising from the PDF, α_s, renormalisation and factorisation scale, and photon-induced uncertainties is drawn. The lower ratio plot shows the influence of the photon-induced corrections on the MSTW2008 prediction, the uncertainty band including only the PDF, α_s and scale uncertainties.

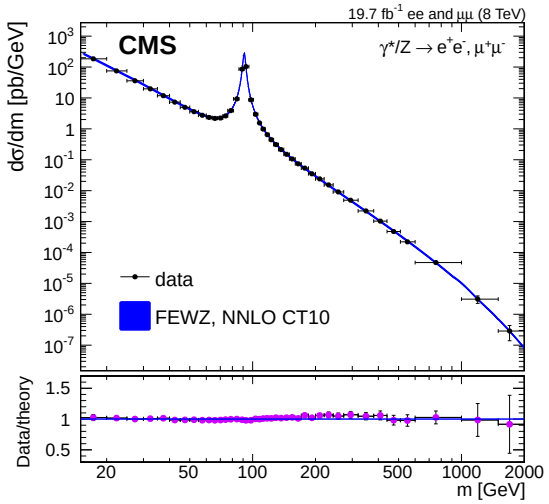

Figure 2. The DY differential cross section as measured in the combined dilepton channel and as predicted by NNLO FEWZ 3.1 with CT10 PDF calculations, for the full phase space.

fusion process contributes about 6% to the total production cross section.

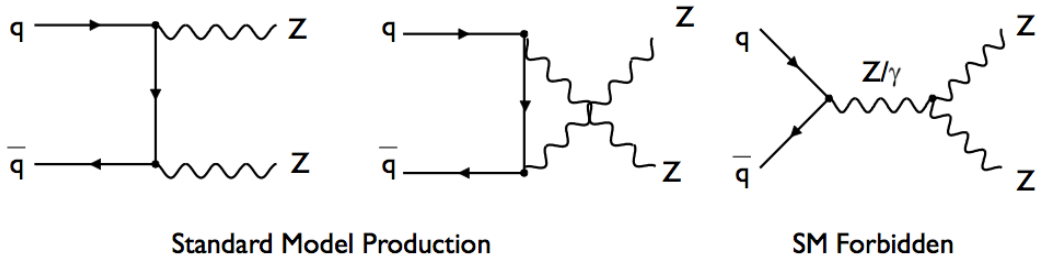

Figure 3. Leading order Feynman diagrams of ZZ production in the dominant $q\bar{q}$ channel. The ZZ production via the s-channel is not allowed in the SM.

Precision measurements use the leptonic decay modes of the Z to reduce the impact of QCD backgrounds. The four lepton final state provides an almost background free signature, at the expense of a relatively small branching ratio $BR(ZZ) \to \ell^+\ell^-\ell^+\ell^- = 0.101^2 \cdot \frac{4}{9} = 0.0045$ [**?**]. The di-lepton and missing energy channel can exploit the one order of magnitude higher branching ratio of $BR(ZZ \to \ell^+\ell^-\nu\bar{\nu}) = 0.101 \cdot 0.20 \cdot 2 \cdot \frac{2}{3} = 0.0269$, at the expense of high background levels.

The ATLAS collaboration has published results on the 7 TeV data-set in the $\ell^+\ell^-\ell^+\ell^-$ and $\ell^+\ell^-\nu\bar{\nu}$ final state [9], and at 13 TeV in the $\ell^+\ell^-\ell^+\ell^-$ final state [10]. The CMS collaboration has analysed the full 7 and 8 TeV data sets in both the $\ell^+\ell^-\ell^+\ell^-$ [11, **?**] and $\ell^+\ell^-\nu\bar{\nu}$ final state [12].

Theoretical predictions for ZZ production are available at NLO in α_s [**?**]. In addition, electroweak corrections at NLO have been calculated [**?**, **?**].

The event selection for the $\ell^+\ell^-\ell^+\ell^-$ final state requires exactly four leptons fulfilling a set of cuts on kinematic quantities. ATLAS and CMS use similar criteria as listed in detail in Table **??**. While ATLAS uses $l = e, \mu$, CMS includes also $Z \to \tau^+\tau^-$ with subsequent hadronic and leptonic τ decays. ATLAS uses in addition forward leptons outside the ID tracker to increase the acceptance by 6% for electrons and 10% for muons. The $\ell^+\ell^-\ell^+\ell^-$ channels offers the cleanest event sample with a background level of only $2-3\%$ from $Z + jets$, , and di-boson events. The background is estimated from data by control regions with looser selection criteria.

Events in the $\ell^+\ell^-\nu\bar{\nu}$ final state are characterized by exactly two leptons and missing energy. The event selection requires a leptonic Z candidate and missing energy in the event. Both experiments used refined observables of missing energy with additional information to improve the rejection against instrumental background. The background level is in the same order as the signal and substantially higher then for $\ell^+\ell^-\ell^+\ell^-$. Main background sources are $V + jets$, and di-boson production. ATLAS and CMS use data driven techniques to constrain the dominant background sources.

Besides the total cross section for the $pp \to ZZ$ production process, both experiments measure also fiducial and differential cross sections. The results are summarized in Tabel 1. ATLAS and CMS use different definitions of the fiducial phase

space which needs to be taken into account to make a direct comparison is possible. For the total cross section a slightly different mass range for the Z mass range is used, where CMS uses a wider range of 60 GeV $< m_Z <$ 120 GeV then ATLAS with 66 GeV $< m_Z <$ 116 GeV, which contributes to the difference in the quoted predicted cross section. Good agreement of experimental and theoretical cross section values is observed.

Experiment	decay channel	$\sqrt{s}$	measured σ_{total} [pb]	predicted σ_{total} [pb]	reference
ATLAS	$\ell^+\ell^-\ell^+\ell^-$, $\ell^+\ell^-\nu\bar{\nu}$	7 TeV	6.7 ± 0.7 (stat.) $^{+0.4}_{-0.3}$ (syst.) ± 0.3 (lumi.)	$6.18^{+0.25}_{-0.18}$	[9]
CMS	$\ell^+\ell^-\ell^+\ell^-$	7 TeV	6.2 $\pm ^{+0.9}_{-0.8}$ (stat.) $^{+0.4}_{-0.3}$ (syst.) ± 0.1 (lumi.)	6.3±0.4	[11]
CMS	$\ell^+\ell^-\nu\bar{\nu}$	7 TeV	5.2 $\pm ^{+1.5}_{-1.4}$ (stat.) $^{+1.4}_{-1.1}$ (syst.) ± 0.2 (lumi.)	6.1±0.3	[11]
CMS	$\ell^+\ell^-\ell^+\ell^-$	8 TeV	7.7 ± 0.5 (stat.) $^{+0.5}_{-0.4}$ (syst.) ± 0.2 (lumi.)	7.7±0.6	[13]
CMS	$\ell^+\ell^-\nu\bar{\nu}$	8 TeV	6.9 ± 0.8 (stat.) $^{+1.8}_{-1.4}$ (syst.) ± 0.3 (lumi.)	7.6±0.3	[11]
ATLAS	$\ell^+\ell^-\ell^+\ell^-$	13 TeV	16.7 $\pm ^{+2.2}_{-2.0}$ (stat.) $^{+0.9}_{-0.7}$ (syst.) $\pm ^{+1.o}_{-0.7}$ (lumi.)	$15.6^{+0.4}_{-0.4}$	[?]

Table 1. Summary of measured ZZ production cross sections from ATLAS and CMS at 7, 8 and 13 TeV centre-of-mass energies in the four lepton and $\ell^+\ell^-\nu\bar{\nu}$ final state.

Limits on ATGC parameters are determined with differential distributions of the invariant di-boson mass (CMS, four lepton channel), the transverse momentum of the leading lepton (CMS, $\ell^+\ell^-\nu\bar{\nu}$-channel), or the transverse momentum of the leading Z(ATLAS, all channels). A comparison of the measured and predicted differential cross sections in the four-lepton invariant mass is shown from CMS in Figure 4. Also shown is the prediction in the presence of a non-zero value of the anomalous coupling parameter $f_4^Z = 0.015$, which shows an enhancement over the SM value at high invariant masses.

Both experiment publish 95% CL limits on ATGC without form factors in the $\ell^+\ell^-\ell^+\ell^-$ and $\ell^+\ell^-\nu\bar{\nu}$ channels. The results are in agreement with the SM and summarized in Figure 5 taken from Ref. [14]. The precision of the LHC results is driven by the steep increase of sensitivity with higher centre-of-mass energy and are about 2 orders of magnitude better compared to the combined LEP result [15].

3.2.2. WZ production At the LHC, $W^\pm Z$ diboson are produced from quark-antiquark initial states at leading order (LO) and quark-gluon initial states at next-to-leading order (NLO). The SM allowed s-channel diagram has a triple boson vertex and is sensitive to anomalous couplings of gauge bosons.

The ATLAS experiment measured the $W^\pm Z$ production cross section in the fully leptonic decay channel $\ell^+\ell^-\ell\nu$ [16] at $\sqrt{s} = 7$ TeV and $\sqrt{s} = 8$ TeV and set limits on anomalous charged TGC. In this analysis the final states involving electrons or muons are considered signal, whereas boson decays to tau's are considered as background. The dominant background sources are Z+jet and ZZ production, constituting about 40% of the background. The overall signal over background ratio is about 3.7. The dominant systematic uncertainty is from the data-driven estimate of the background, where the dominant Z + jets contributes with (±3.8%).

The fiducial cross section defined by $p_{\mathrm{T}}^{\mu,e} > 15$ GeV for the leptons from the Z decay, $p_{\mathrm{T}}^{\mu,e} > 20$ GeV for the lepton from the W, $|\eta^{\mu,e}| < 2.5$, $p_{\mathrm{T}}^{\nu} > 25$ GeV,

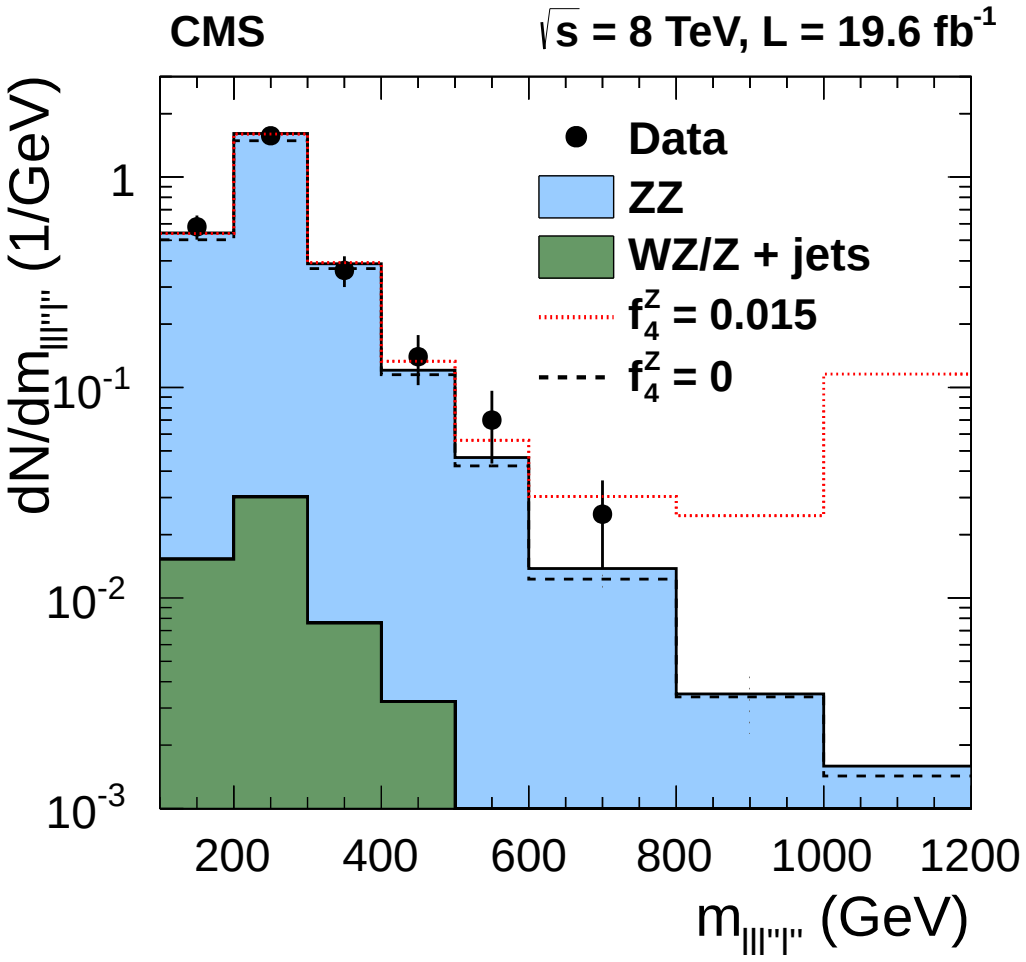

Figure 4. Distribution of the four-lepton reconstructed mass for the combined $4e$, 4μ, and $2e2\mu$ channels from CMS [**?**]. Points represent the data, the shaded histogram labeled ZZ represents the predictions for ZZ signal, the histograms labeled $W^{\pm}Z/Z$+jets shows background estimated form data. The dashed and dotted histograms indicate the SM expectation (f4Z = 0) and in the presence of an ATGC (f4Z = 0.015) with all the other anomalous couplings set to zero. The last bin includes all entries with masses above 1000 GeV.

$|m_l l - m_Z| < 10$ GeV, $M_T^W > 20GeV$ and $\Delta R > 0.3$ for the three possible $\ell\ell$ pairings. The total cross section requires the mass of the Z to be in the range of 66 GeV $< |m_Z| <$ 116 GeV to suppress the contribution from γ^*. The fiducial and total cross sections are compared to the SM expectation at NLO in Table 3.2.2.

In Figure 7 the differential cross section measured in bins of p_{T}^Z is shown, compared to SM prediction and a set of anomalous TGC couplings. The normalized p_{T}^Z spectrum is unfolded and compared to the NLO calculation of MC@NLO in Figure 7, showing good agreement with the SM.

Limits on the charged ATGC parameters $\Delta\kappa_Z$, λ_Z and g_1^Z are extracted from the transverse momentum distribution of the Z, p_{T}^Z [16] or from the transverse mass of

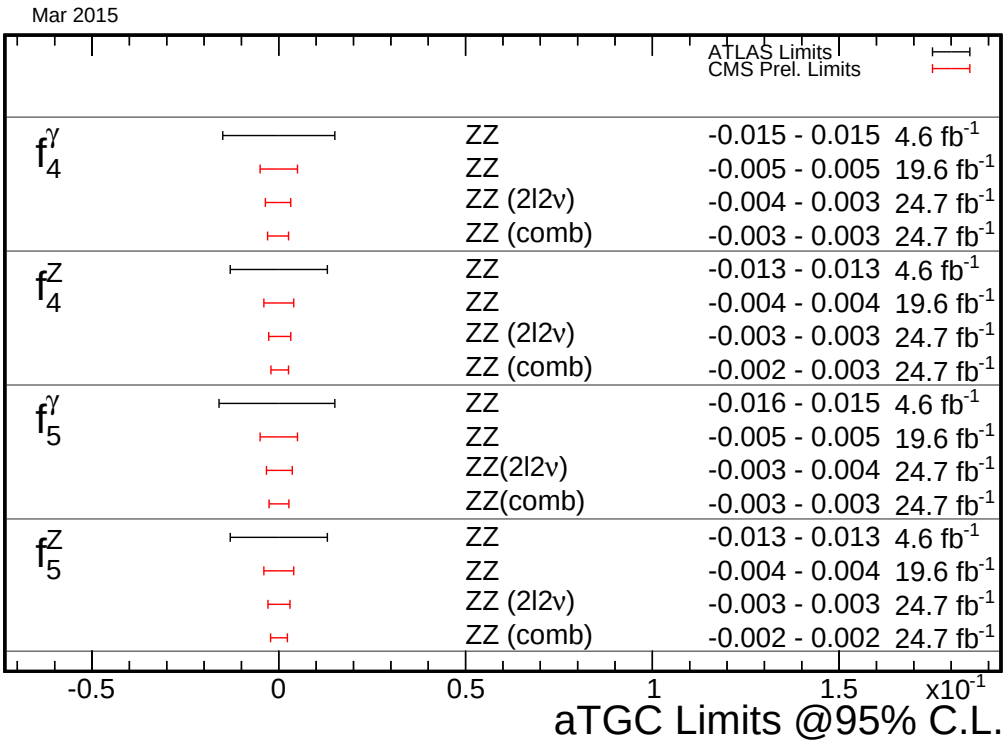

Figure 5. Comparison of the limits on f_{40}^V and f_{50}^V from ATLAS and CMS in the $\ell^+\ell^-\ell^+\ell^-$ and $\ell^+\ell^-\nu\bar{\nu}$ channel at 7 and 8 TeV.

Experiment	cross section	$\sqrt{s}$	measured	predicted	reference
ATLAS	total	7 GeV	$19^{+1.4}_{-1.3}$ (stat.) $\pm$0.9 (syst.) $\pm$ 0.4 (lumi.) pb	17.6 $^{+1.1}_{-1.0}$ pb	[16]
ATLAS	total	8 GeV	24.3$\pm$0.6 (stat.) $\pm$0.6 (syst.) $\pm$0.4 (theo.) $\pm$ 0.5 (lumi.) pb	21.0 $\pm$ 1.6 pb	[17]
ATLAS	fiducial	7 GeV	92 $\pm$ $^{+7}_{-6}$ (stat.) $\pm$4 (syst.) $\pm$ 2 (lumi.) fb	–	[16]
ATLAS	fiducial	8 GeV	92 $\pm$ $^{+7}_{-6}$ (stat.) $\pm$4 (syst.) $\pm$ 2 (lumi.) fb	–	[17]

Table 2. Summary of measured fiducial and total $W^\pm Z$ production cross sections from ATLAS at 7 TeV centre-of-mass energies in the $\ell^+\ell^-\ell\nu$ final state.

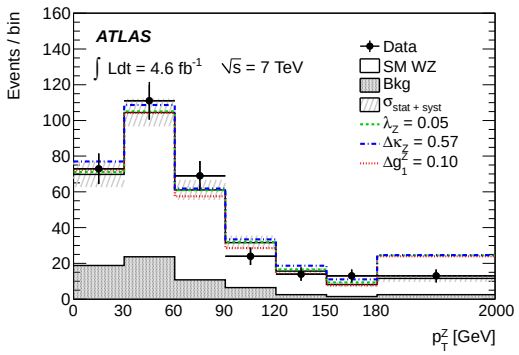

Figure 6. ATLAS measurement of the transverse momentum of the Zin $W^\pm Z$ events (p_{T}^Z) compared with the SM prediction at $\sqrt{s} = 7$ TeV. For illustration calculations for a set of anomalous couplings values are also shown. The full uncertainty contains statistical and systematic uncertainties.

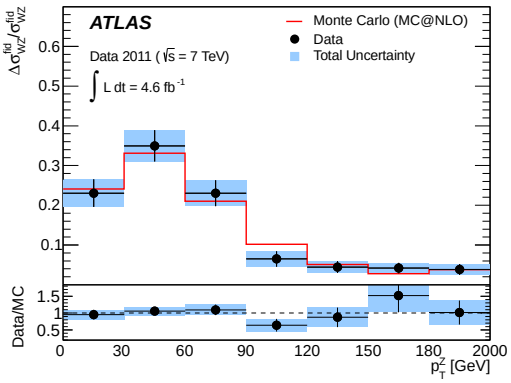

Figure 7. ATLAS measurement of the normalized fiducial cross-sections in bins of p_{T}^{Z} compared with the SM prediction at $\sqrt{s} = 7$ TeV. The full uncertainty contains statistical and systematic uncertainties.

Λ	Coupling	Expected	Observed
2 TeV	g_1^Z	$[-0.023, 0.055]$	$[-0.029, 0.050]$
2 TeV	$\Delta\kappa_Z$	$[-0.17, 0.25]$	$[-0.19, 0.30]$
2 TeV	λ_Z	$[-0.016, 0.016]$	$[-0.016, 0.016]$

Table 3. Expected and observed 95% CL on $\Delta\kappa_Z$, λ_Z and g_1^Z for a cut-off parameter $\Lambda = 2$ TeV and $\Lambda = \infty$.

the WZ system [17]. The ATGC parameter 95% CL limits using a dipole form-factor with a cut-off of $\Lambda = 2$ TeV and without a form-factor are quoted in Table 5 from the statistically more precise 8 TeV data set analysis [17].

3.2.3. WW production The W^+W^- production process has the highest production cross section among the massive vector diboson processes. It is also an important background process to Higgs production and to searches for new physics. ATLAS and CMS, observed the W^+W^- production process in the fully leptonic channel and published results for 7 TeV (ATLAS [18], CMS [19]) and 8 TeV (CMS [20]) centre-of-mass energy. Three final states, namely ee, $\mu\mu$, and $e\mu$ are included in the analyses. The contribution from leptonically decaying τ leptons is included in the signal definition. Although the production cross section is relatively high, the signature of two opposite sign leptons and missing transverse energy is shared with many processes and a careful control of the backgrounds is necessary to achieve a precise measurement.

Candidate W^+W^- events are selected by by requiring two oppositely charged leptons accompanied with large $E_{\mathrm{T}}^{\mathrm{miss}}$. The dominant background sources are $t\bar{t}$ and single top quark, $W^{\pm}$/+jets, followed by Z/γ^*+jets production. To suppress the dominant $t\bar{t}$ background, events with one or more jets are rejected. Additional requirements on $E_{\mathrm{T}}^{\mathrm{miss}}$ and the use of top quark-taggers further reduce the residual

background to about 30%. The dominant systematic uncertainty is related to the jet veto efficiency and estimated to about 5% for the W^+W^- production. The experiments quote a theoretical uncertainties on the signal acceptance due to variations of the parton distribution functions and renormalisation and factorization scale in the range of 1-2%.

Both ATLAS and CMS provide a measurement of the total cross section for the process $pp \to W^+W^-$ and compare to theoretical calculations. The Higgs process contributes with about 4% to the total cross section and has not been taken into account in the comparison to the SM predictions. The total cross section results are summarised in Table 3.2.3. A good agreement of the experiments for the measured cross section as well as for the theoretical predictions is observed. A normalised differential measurement of the fiducial cross section in bins of p_{T} of the leading lepton is presented by ATLAS, as shown in Figure 8. The unfolded spectrum is in agreement with the SM prediction.

Experiment	cross section	$\sqrt{s}$	measured	predicted	reference
ATLAS	total	7 GeV	51.9 $\pm$2.0 (stat.) 3.9 (syst.) $\pm$ 2.0 (lumi.) pb	44.7 $^{+2.1}_{-1.9}$ pb	[18]
CMS	total	7 GeV	52.4 $\pm$2.0 (stat.) 4.5 (syst.) $\pm$ 1.2 (lumi.) pb	47.0 $\pm$2.0 pb	[19]
CMS	total	8 GeV	69.9 $\pm$2.8 (stat.) 5.6 (syst.) $\pm$ 3.1 (lumi.) pb	57.3 $^{+2.3}_{-1.6}$ pb	[19]

Table 4. Summary of measured fiducial and total W^+W^- production cross sections from ATLAS and CMS at 7 and 8 TeV centre-of-mass energies in the $\ell\nu\ell\nu$ final state.

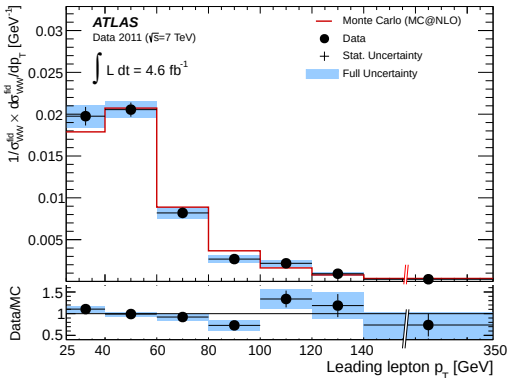

Figure 8. ATLAS measurement of the transverse momentum of the leading lepton in W^+W^- events compared with the SM prediction at $\sqrt{s} = 7$ TeV. The full uncertainty contains statistical and systematic uncertainties.

The leading lepton p_{T} spectrum of the W^+W^- process is sensitive to anomalous gauge boson coupling parameters $\Delta\kappa_\gamma$, $\Delta\kappa_Z$, λ_γ, λ_Z, and Δg_1^Z. Both ATLAS and CMS quote limits in the LEP parametrization [21] that introduces $SU(2) \times U(1)$ gauge invariance constraints to reduce the number of free parameters to Δg_1^Z, $\Delta\kappa_\gamma$, and λ_Z. The obtained limits assuming no form-factor are compared for both expected and measured 95% CL limits in Table 5.

	Observed (CMS)	Observed (ATLAS)	Expected (ATLAS)
Δg_1^Z	$[-0.095, 0.095]$	$[-0.039, 0.052]$	$[-0.039, 0.052]$
$\Delta\kappa_\gamma$	$[-0.21, 0.22]$	$[-0.14, 0.14]$	$[-0.13, 0.13]$
λ_Z	$[-0.048, 0.048]$	$[-0.062, 0.059]$	$[-0.060, 0.059]$

Table 5. Expected and observed 95% CL limits on the ATGC parameters $\Delta\kappa_\gamma$, λ_Z and Δg_1^Z in the LEP parametrization derived from the leading lepton p_{T} spectrum in W^+W^- production at 7 TeV (ATLAS [18],CMS [19]). No form-factor is applied to the ATGC parameters.

3.2.4. Semi-leptonic VV production The cross sections for W^+W^- and $W^\pm Z$ production have been measured also in the semileptonic decay channel in the $W^\pm V \to \ell^\pm\nu q\bar{q}$ final state with $V = W^\pm, Z$. The semileptonic final state has a relatively large background mainly from V production with associated jets compared to the fully leptonic decay channels, but offers a substantially larger branching fraction. The increased statistics of signal events at high partonic centre of mass compared to the fully leptonic decay modes enhances specifically the sensitivity to aTGC. ATLAS and CMS have published measurements of the inclusive production cross section $W^+W^- + W^\pm Z$ and set limits on charged aTGC with the full data set of the $\sqrt{s} = 7$ TeV run [22, 23].

Both analysis use the semileptonic decay channel with an electron or muon and two jets in the final state. The event selection sets requirements on the lepton p_{T}, the $E_{\mathrm{T}}^{\mathrm{miss}}$, di-jet invariant mass, and the event topology. The signal fraction of $W^+W^- + W^\pm Z$ in the event sample after selection is only about 1%, and no further selection criteria are applied to distinguish between W^+W^- and $W^\pm Z$ production. The dominant background from $Z/W^\pm$+jets production is constrained with data driven methods, folowed by the sub-leading background contributions from $t\bar{t}$ and multi-jet production. The cross-section is extracted with a simultaneous fit of the di-jet invariant mass spectrum comprising the signal and background components. In Figure 9 the di-jet invariant mass spectrum and the extracted signal after background subtraction from Ref. [22] is shown. The largest systematic uncertainty is related to the modelling of the $Z/W^\pm$+jets background with about 20% on the cross section.

The measured and predicted cross sections are compared in Table 3.2.4.

Experiment	cross section	$\sqrt{s}$	measured	predicted	reference
ATLAS	total	7 GeV	68±7 (stat.) ±19 (syst.+lumi.) pb	61.1 ± 2.2 pb	[22]
CMS	total	7 GeV	68.9 ± ±8.7 (stat.) ±9.7 (syst.) ± 1.5 (lumi.) pb	65.6 ± 2.2 pb	[23]

Table 6. Summary of measured total $W^\pm Z + W^+W^-$ production cross sections from ATLAS and CMS at 7 TeV centre-of-mass energies in the $W^\pm V \to \ell^\pm\nu q\bar{q}$ final state.

To extract limits on aTGC parameters the transverse momentum of the di-jet system $p_{\mathrm{T}}(jj)$ is used by ATLAS and CMS. The resulting 95% CL limits are listed in Table 7. The ATLAS limits use the LEP scenario [21], while the CMS limits are derived in the HISZ [24, 25] scenario. The achieved precision is comparable to the fully leptonic

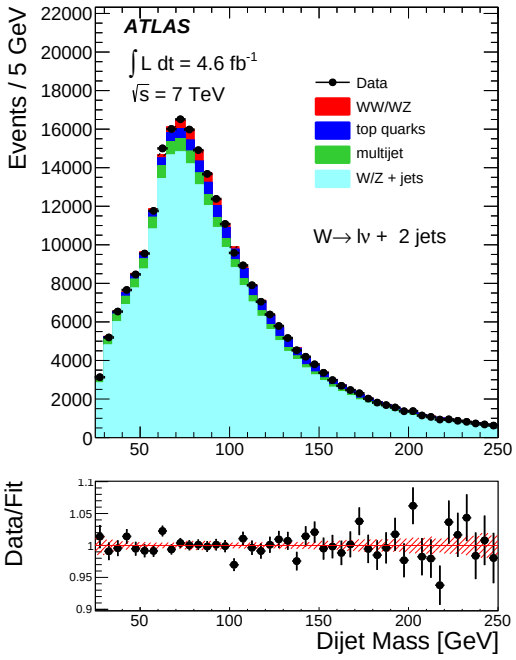

(a)

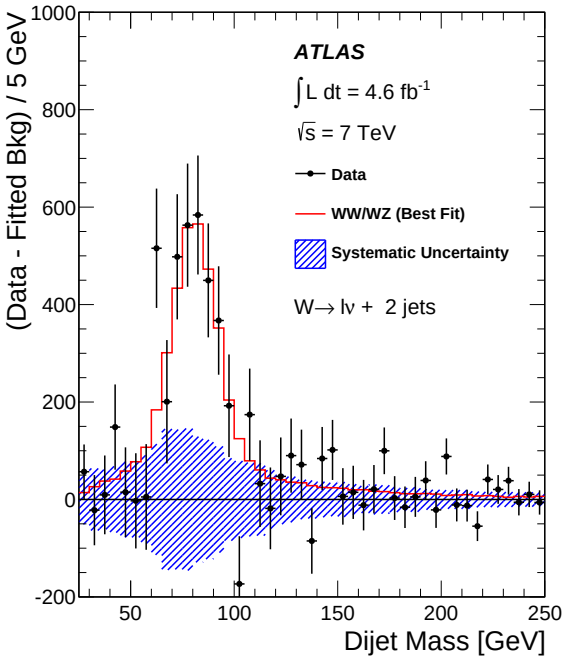

(b)

Figure 9. (a) The di-jet invariant mass spectrum for the sum of electron and muon channels, (b) the distribution of the background subtracted data. The lower panel shows that ratio of data and total fit result.

channel.

A measurement of the $W^{\pm}Z$ and ZZ production cross sections at $\sqrt{s} = 8$ TeV with a data set of 18.9 fb^{-1} in the semileptonic final state with two b-quark jets

	CMS	ATLAS	
	Observed	Observed	Expected
$\lambda_Z = \lambda_\gamma$	$[-0.038, 0.030]$	$[-0.039, 0.040]$	$[-0.048, 0.047]$
$\Delta\kappa_\gamma$	$[-0.11, 0.14]$	$[-0.21, 0.22]$	$[-0.23, 0.25]$
Δg_1^Z	–	$[-0.055, 0.071]$	$[-0.072, 0.085]$

Table 7. Expected and observed 95% CL on $\Delta\kappa_\gamma$, $\lambda_Z = \lambda_\gamma$ and Δg_1^Zin measured in the $W^\pm V \to \ell^\pm\nu q\bar{q}$ final state from the ATLAS [22] and CMS [23] collaborations.

from the $Z$and $\ell^+\ell^-$, $\nu\bar{\nu}$ or $\ell\nu$ has been published by CMS [26], so far the only published results at 8 TeV for these channels. The measured cross sections ($\sigma(pp \to W^\pm Z) = 30.7 \pm 9.3(\text{stat}) \pm 7.1(\text{syst}) \pm 4.1(\text{theo}) \pm 1.0(\text{lumi})$pb and $\sigma(pp \to ZZ) = 6.5 \pm 1.7(\text{stat}) \pm 1.0(\text{syst}) \pm 0.9(\text{theo}) \pm 0.2(\text{lumi})$pb) are consistent with theoretical calculation at NLO in α_s ($\sigma(pp \to ZZ) = 22.3 \pm 1.1$pb and $\sigma(pp \to ZZ) = 7.7 \pm 0.4$pb), with the precision being still statistically limited.

3.2.5. Leptonic $V\gamma$ production The di-boson system of a massive vector boson and a photon has a similar electroweak production rate as the massive di-boson final states. Initial and final state QED radiation of photons from the incoming quarks and outgoing charged decay products are dominating the total cross section for this final state. To compare to theory fiducial cross sections are defined, that enhance the electroweak component. The $W^\pm\gamma$ process has been studied in the leptonic decay $W^\pm\gamma \to \ell^\pm\nu\gamma$ and limits on charged aTGC are set. The $Z\gamma$ process has two leptonic decay modes $Z\gamma \to \ell^+\ell^-\gamma$ and $Z\gamma \to \nu\bar{\nu}\gamma$, which are both sensitive to neutral aTGC. Due to the absence of final state radiation in $Z \to \nu\bar{\nu}$ and the about two times higher branching ratio compared to $Z \to \ell^+\ell^-$ the $\nu\bar{\nu}$ final state is more sensitive to aTGC. The main background arrises from $W^\pm$+jets and Z+jets production, where one jet is misidentified as an isolated photon. Data driven techniques are employed to estimate this background. Other important sources of backgrounds are multi-jet production and $t\bar{t}$ pair production in association with a photon, and are estimated from simulation. The achieved signal to background ratios range from about 0.8 – 1.5 for $W^\pm\gamma \to \ell^\pm\nu\gamma$ to 3.5 – 7 for $Z \to \ell^+\ell^-$ depending on channel and experiment.

ATLAS and CMS have published measurements of fiducial production cross sections of $W^\pm\gamma \to \ell^\pm\nu\gamma$, $Z\gamma \to \ell^+\ell^-\gamma$ at $\sqrt{s} = 7$ TeV and $\sqrt{s} = 8$ TeV. The fiducial volume is defined at particle level with kinematic selection criteria on objects and at the event level. ATLAS and CMS differ in the definitions of the fiducial cross section, leading to differences in the predicted cross sections and making a direct comparison difficult. The cross-section for $Z\gamma \to \ell^+\ell^-\gamma$ and $W^\pm\gamma \to \ell^\pm\nu\gamma$ is defined as $p_{\text{T}}(\gamma) > 15$ GeV,$\Delta(\ell, \gamma) > 0.7$, and additionally for $Z\gamma$ $m(\ell\ell) > 50(40)$ GeV) for CMS (ATLAS). ATLAS further requires $|\eta(\ell)| < 2.47$, $|\eta(\gamma)| < 2.37$, and $E_{\text{T}}(jet) > 30$ GeV, $|\eta(jet)| < 4.4$, $\Delta R(jet, x) > 0.3$ for jets. For the $Z\gamma \to \nu\bar{\nu}\gamma$ process the cross section is defined as $E_{\text{T}}(\gamma) > 145(100, 130)$ GeV, $|\eta(\gamma)| < 1.4(2.37)$, $p_{\text{T}}(\nu\nu) > 130(90, 100)$ for

CMS (ATLAS 7 TeV [27], and 8 TeV [28]). A summary of the measurements is given in Table 3.2.5. Overall the agreement of the measured and NLO predicted cross sections is good.

Experiment	process	cross section	$\sqrt{s}$	measured	predicted	reference
ATLAS	$W^{\pm}\gamma \to \ell^{\pm}\nu\gamma$	inclusive	7 GeV	2.77 ± 0.03 (stat) ± 0.33 (syst) ± 0.14 (lumi) pb	1.96 ± 0.17 pb	[29]
ATLAS	$W^{\pm}\gamma \to \ell^{\pm}\nu\gamma$	exclusive	7 GeV	1.76 ± 0.03 (stat) ± 0.21 (syst) ± 0.08 (lumi) pb	1.39 ± 0.13 pb	[29]
ATLAS	$Z\gamma \to \ell^{+}\ell^{-}\gamma$	inclusive	7 GeV	1.31 ± 0.02 (stat) ± 0.11 (syst) ± 0.05 (lumi) pb	1.18 ± 0.05 pb	[29]
ATLAS	$Z\gamma \to \ell^{+}\ell^{-}\gamma$	exclusive	7 GeV	1.05 ± 0.02 (stat) ± 0.10 (syst) ± 0.04 (lumi) pb	1.06 ± 0.05 pb	[29]
ATLAS	$Z\gamma \to \nu\bar{\nu}\gamma$	inclusive	7 GeV	0.133 ± 0.013 (stat) ± 0.020 (syst) ± 0.005 (lumi) pb	0.156 ± 0.012 pb	[27]
ATLAS	$Z\gamma \to \nu\bar{\nu}\gamma$	exclusive	7 GeV	0.116 ± 0.010 (stat) ± 0.013 (syst) ± 0.004 (lumi) pb	0.115 ± 0.009 pb	[27]
CMS	$Z\gamma \to \ell^{+}\ell^{-}\gamma$	inclusive	7 GeV	5.33 ± 0.08 (stat) ± 0.25 (syst) ± 0.12 (lumi) pb	5.45 ± 0.27 pb	[30]
CMS	$W^{\pm}\gamma \to \ell^{\pm}\nu\gamma$	inclusive	7 GeV	37.0 ± 0.8 (stat) ± 4.0 (syst) ± 0.8 (lumi) pb	31.8 ± 1.8 pb	[30]
CMS	$Z\gamma \to \nu\bar{\nu}\gamma$	inclusive	7 GeV	21.1 ± 4.2 (stat.) ± 4.3 (syst) ± 0.5 (lumi) fb	21.9 ± 1.1 fb	[27]
ATLAS	$Z\gamma \to \ell^{+}\ell^{-}\gamma$	inclusive	8 GeV	1.51 ± 0.01 (stat) ± 0.08 (syst) ± 0.03 (lumi) pb	1.35 ± 0.07 pb	[28]
ATLAS	$Z\gamma \to \ell^{+}\ell^{-}\gamma$	exclusive	8 GeV	1.19 ± 0.01 (stat) ± 0.07 (syst) ± 0.02 (lumi) pb	1.19 ± 0.08 pb	[28]
ATLAS	$Z\gamma \to \nu\bar{\nu}\gamma$	inclusive	8 GeV	68 ± 4 (stat) ± 32 (syst) ± 1 (lumi) fb	68 ± 2 fb	[28]
ATLAS	$Z\gamma \to \nu\bar{\nu}\gamma$	exclusive	8 GeV	43 ± 2 (stat) ± 10 (syst) ± 1 (lumi) fb	51 ± 2 fb	[28]
CMS	$Z\gamma \to \ell^{+}\ell^{-}\gamma$	inclusive	8 GeV	2063 ± 19 (stat) ± 98 (syst) ± 54 (lumi) fb	2100 ± 120 fb	[31]
CMS	$Z\gamma \to \ell^{+}\ell^{-}\gamma$	exclusive	8 GeV	1770 ± 18 (stat) ± 115 (syst) ± 46 (lumi) fb	1800 ± 120 fb	[31]
CMS	$Z\gamma \to \nu\bar{\nu}\gamma$	inclusive	8 GeV	52.7 ± 2.1 (stat) ± 6.4 (syst) ± 1.4 (lumi) fb	40.7 ± 4.9 fb	[32]

Table 8. Summary of measured $V\gamma$ production cross sections from ATLAS and CMS at 7 and 8 TeV centre-of-mass energies in the $W^{\pm}\gamma \to \ell^{\pm}\nu\gamma$, $Z\gamma \to \nu\bar{\nu}\gamma$ and $Z\gamma \to \ell^{+}\ell^{-}\gamma$ final states. The inclusive cross section is for $n_{jet} \geq 0$ and the exclusive cross section is for $n_{jet} = 0$. The cross section definitions differ for ATLAS and CMS and the numerical values are not directly comparable. For the $Z\gamma \to \nu\bar{\nu}\gamma$ process ATLAS uses a different cross section definition between the 7 TeV and 8 TeV measurements.

To extract limits on aTGC parameters the transverse momentum of the photon $p_{\mathrm{T}}(\gamma)$ is used by CMS, while ATLAS uses a more conservative approache by combining the observed number of exclusive $V\gamma$ candidate events with $E_{\mathrm{T}}(\gamma) > 100$ GeV. The channel most sensitive to the neutral TGC couplings h_{30}^{V}, $h_{40}^{V}$is $Z\gamma \to \nu\bar{\nu}\gamma$ due to the high branching ratio of Z to neutrinos of 20%. Figure 10 shows the transverse momentum of the photon for at 8 TeVmeasured by CMS in the $Z\gamma \to \nu\bar{\nu}\gamma$ channel [32] together with a hypothetics TGC signal.

The resulting 95% CL limits for charged ($W^{\pm}\gamma$) and neutral ($Z\gamma$) TGC are listed in Table 9. For comparison only limits obtained without the use of a form factor are listed. ATLAS also provides limits with unitarity preserving form factors, and in case of the 8 TeV analysis limits as a function of $\Lambda_F F$ [28].

3.3. Inclusive tri-boson production

One avenue for testing quartic gauge boson interactions is through inclusive tri-boson production: $pp \to VV'V''$ for $V = \gamma, W, Z$. Using the Run 1 data sample, the triply heavy such channels (WWW, WWZ, WZZ, ZZZ) are not accessible anywhere near SM rates, due to their small 8 TeV cross sections and comparably large multi-lepton backgrounds. The photonic channels do not suffer as much from these problems, and sensitivity is at or near SM rates in Run 1.

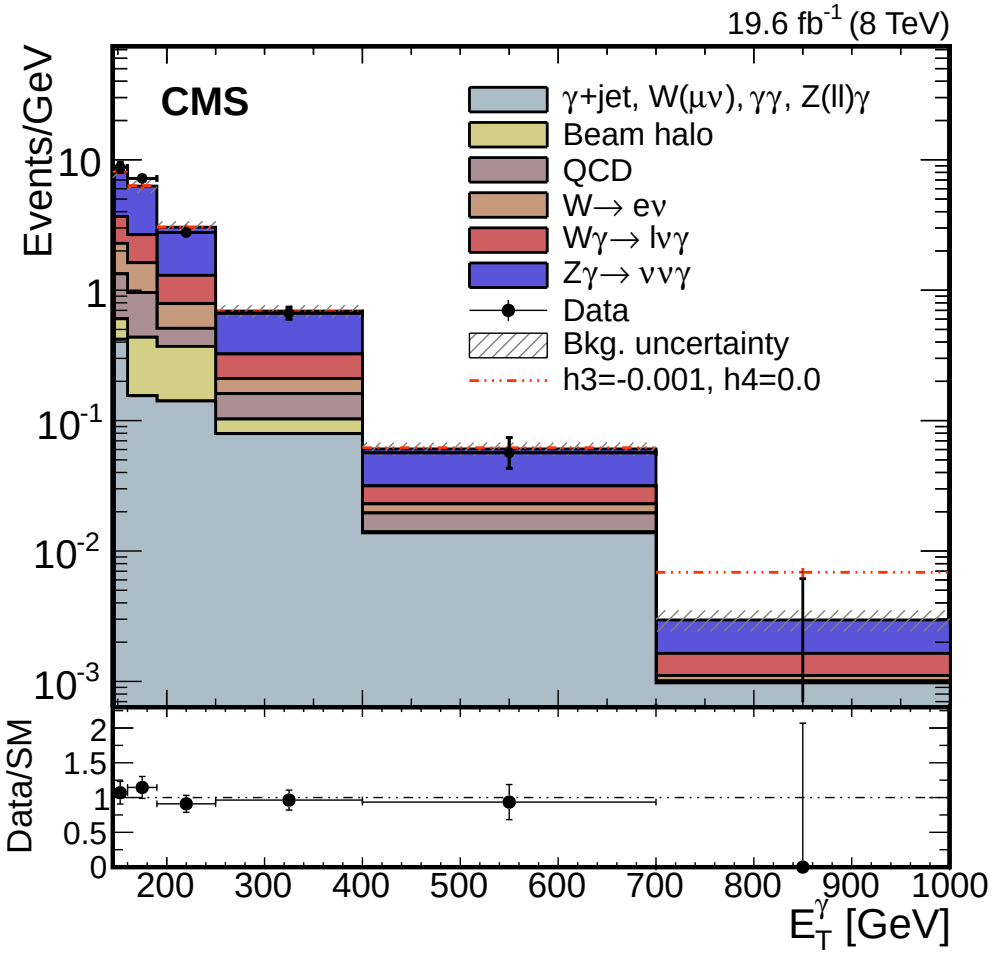

Figure 10. The $E_{\mathrm{T}}(\gamma)$ distribution from CMS [32] in data (points) compared to signal and estimated background contributions (histogram). A aTGC signal with $h_{30}^{V} = -0.001$ is shown for comparison with the dot-dashed histogram. The background uncertainty includes statistical and systematic contributions.

An ATLAS analysis [33] has found evidence for $W\gamma\gamma$ production. In this process, a W is produced in the hard quark scattering, and the two photons can originate from either initial- or final-state radiation, or interaction with the W via triple or quartic gauge boson interactions. Events are selected with lepton $p_{\mathrm{T}} > 20$ GeV, $E_{\mathrm{T}}^{\mathrm{miss}} > 25$ GeV, $m_T > 40$ GeV and two photons with $p_{\mathrm{T}} > 20$ GeV. Minimum angular separations between the lepton and photons are also required to reduce the contribution of final-state radiation amplitudes, which do not probe gauge boson interactions. This selection results in 157 events in the 8 TeV data. Roughly half of these events are backgrounds: W or $W\gamma$ plus jets production with jets misidentified as photons, $Z\gamma$ events with leptons misidentified as photons, or $\gamma\gamma$ plus jets events with jets misidentified as leptons. The backgrounds are estimated for electron and muon events separately via template fits to photon isolation distributions in data (W or $W\gamma$ plus jets) or lepton isolation distributions in data ($Z\gamma$ or $\gamma\gamma$ plus jets).

	Process	$\sqrt{s}$	$\mathcal{L}$[fb^{-1}] ATLAS, CMS	ATLAS Observed	ATLAS Expected	CMS Observed
$\Delta\kappa_\gamma$	$W^\pm\gamma \to \ell^\pm\nu\gamma$	7 TeV	4.6 fb^{-1}, 5 fb^{-1}	$[-0.41, 0.46]$	$[-0.38, 0.43]$	$[-0.38, 0.29]$
λ_γ	$W^\pm\gamma \to \ell^\pm\nu\gamma$	7 TeV	4.6 fb^{-1}, 5 fb^{-1}	$[-0.065, 0.061]$	$[-0.060, 0.056]$	$[-0.050, 0.037]$
h_{30}^γ	$Z\gamma \to \ell^+\ell^-\gamma$,$Z\gamma \to \nu\bar{\nu}\gamma$	7 TeV	4.6 fb^{-1}, 5 fb^{-1}	$[-0.015, 0.016]$	$[-0.017, 0.018]$	$< 2.9 \cdot 10^{-3}$
h_{30}^Z	$Z\gamma \to \ell^+\ell^-\gamma$,$Z\gamma \to \nu\bar{\nu}\gamma$	7 TeV	4.6 fb^{-1}, 5 fb^{-1}	$[-0.013, 0.014]$	$[-0.015, 0.016]$	$< 2.7 \cdot 10^{-3}$
h_{40}^γ	$Z\gamma \to \ell^+\ell^-\gamma$,$Z\gamma \to \nu\bar{\nu}\gamma$	7 TeV	4.6 fb^{-1}, 5 fb^{-1}	$[-9.4 \cdot 10^{-5}, 9.2 \cdot 10^{-5}]$	$[-1.0 \cdot 10^{-4}, 1.0 \cdot 10^{4}]$	$< 1.5 \cdot 10^{-5}$
h_{40}^Z	$Z\gamma \to \ell^+\ell^-\gamma$,$Z\gamma \to \nu\bar{\nu}\gamma$	7 TeV	4.6 fb^{-1}, 5 fb^{-1}	$[-8.7 \cdot 10^{-5}, 8.7 \cdot 10^{-5}]$	$[-9.7 \cdot 10^{-5}, 9.7 \cdot 10^{5}]$	$< 1.3 \cdot 10^{-5}$
h_{30}^γ	$Z\gamma \to \ell^+\ell^-\gamma$,$Z\gamma \to \nu\bar{\nu}\gamma$	8 TeV	20.3 fb^{-1}, –	$[-9.5 \cdot 10^{-4}, 9.9 \cdot 10^{-4}]$	$[-1.8 \cdot 10^{-3}, 1.8 \cdot 10^{-3}]$	–
h_{30}^Z	$Z\gamma \to \ell^+\ell^-\gamma$,$Z\gamma \to \nu\bar{\nu}\gamma$	8 TeV	20.3 fb^{-1}, –	$[-7.8 \cdot 10^{-4}, 8.6 \cdot 10^{-4}]$	$[-1.5 \cdot 10^{-3}, 1.5 \cdot 10^{-3}]$	–
h_{40}^γ	$Z\gamma \to \ell^+\ell^-\gamma$,$Z\gamma \to \nu\bar{\nu}\gamma$	8 TeV	20.3 fb^{-1}, –	$[-3.2 \cdot 10^{-6}, 3.2 \cdot 10^{-6}]$	$[-6.0 \cdot 10^{-6}, 5.9 \cdot 10^{-6}]$	–
h_{40}^Z	$Z\gamma \to \ell^+\ell^-\gamma$,$Z\gamma \to \nu\bar{\nu}\gamma$	8 TeV	20.3 fb^{-1}, –	$[-3.0 \cdot 10^{-6}, 2.9 \cdot 10^{-6}]$	$[-5.5 \cdot 10^{-6}, 5.4 \cdot 10^{-6}]$	–
h_{30}^γ	$Z\gamma \to \ell^+\ell^-\gamma$	8 TeV	–, 19.5 fb^{-1}	–	–	$[-4.6 \cdot 10^{-3}, 4.6 \cdot 10^{-3}]$
h_{30}^Z	$Z\gamma \to \ell^+\ell^-\gamma$	8 TeV	–, 19.5 fb^{-1}	–	–	$[-3.8 \cdot 10^{-3}, 3.7 \cdot 10^{-3}]$
h_{40}^γ	$Z\gamma \to \ell^+\ell^-\gamma$	8 TeV	–, 19.5 fb^{-1}	–	–	$[-3.6 \cdot 10^{-5}, 3.5 \cdot 10^{-5}]$
h_{40}^Z	$Z\gamma \to \ell^+\ell^-\gamma$	8 TeV	–, 19.5 fb^{-1}	–	–	$[-3.1 \cdot 10^{-5}, 3.0 \cdot 10^{-5}]$
h_{30}^γ	$Z\gamma \to \nu\bar{\nu}\gamma$	8 TeV	–, 19.5 fb^{-1}	–	–	$[-1.1 \cdot 10^{-3}, 0.9 \cdot 10^{-3}]$
h_{30}^Z	$Z\gamma \to \nu\bar{\nu}\gamma$	8 TeV	–, 19.5 fb^{-1}	–	–	$[-1.5 \cdot 10^{-3}, 1.6 \cdot 10^{-3}]$
h_{40}^γ	$Z\gamma \to \nu\bar{\nu}\gamma$	8 TeV	–, 19.5 fb^{-1}	–	–	$[-3.8 \cdot 10^{-6}, 4.3 \cdot 10^{-6}]$
h_{40}^Z	$Z\gamma \to \nu\bar{\nu}\gamma$	8 TeV	–, 19.5 fb^{-1}	–	–	$[-3.9 \cdot 10^{-6}, 4.5 \cdot 10^{-6}]$

Table 9. Expected and observed 95% CL on h_{30}^γ, h_{30}^Z, h_{40}^γ, and h_{40}^Z measured in the $Z\gamma \to \ell^+\ell^-\gamma$ and $Z\gamma \to \nu\bar{\nu}\gamma$ final states from the ATLAS and CMS collaborations.

The diphoton invariant mass distributions of selected events, along with estimated backgrounds, are shown in Fig. 11. A signal excess is observed in both lepton channels, corresponding to a combined significance larger than 3σ. The fiducial production cross section is estimated for both the inclusive case and an exclusive selection with a jet veto for jets with $p_{\mathrm{T}} > 30$ GeV, similar to the ATLAS $W\gamma$ and $Z\gamma$ analysis. The measured inclusive cross section, $6.1^{+1.1}_{1.0}(\mathrm{stat.}) \pm 1.2(\mathrm{syst.}) \pm 0.2(\mathrm{lumi.})$ fb, is 1.9σ higher than a NLO prediction from MCFM of 2.90 ± 0.16 fb. The exclusive cross section, $2.9^{+0.8}_{0.7}(\mathrm{stat.})^{+1.0}_{0.9}(\mathrm{syst.}) \pm 0.1(\mathrm{lumi.})$ fb, agrees with the MCFM prediction of 1.88 ± 0.20 fb. A similar phenomenon was observed in the $W\gamma/Z\gamma$ analysis, where it is believed missing higher order corrections to the inclusive cross section are substantial. Systematic uncertainties for these cross sections are predominantly from the data-driven background estimation methods.

The exclusive $W\gamma\gamma$ event yield at high diphoton mass ($m_{\gamma\gamma} > 300$ GeV) is used to obtain 95% CL bounds on dimension 8 EFT couplings $f_{T,0}$ and $f_{M,(2,3)}$ [34]. For the case of no unitarizing form factor, the observed limit on $|f_{T,0}/\Lambda^4|$ is 90 TeV^{-4}. For a unitarizing form factor with a cutoff scale of 600 GeV, these limits are relaxed by up to a factor of 8.

CMS has performed a search for $WV\gamma$ production in 8 TeV data [35], where V is a hadronically decaying W or Z. This process is sensitive to the $WW\gamma\gamma$ and $WWZ\gamma$ quartic gauge boson interactions, as depicted in Fig. 12. W candidates are selected by requiring either one muon ($P_T > 25$ GeV and $|\eta| < 2.1$) or one electron ($P_T > 30$ GeV and $|\eta| < 2.5$), missing transverse energy in excess of 35 GeV, and vetoes on additional leptons with $P_T > 10(20)$ GeV for muons (electrons). Photon candidates are required to have $E_T > 30$ GeV and $|\eta| < 1.44$; the central η restriction selects for higher purity photons. The third V boson is selected from jet pairs with jet $E_T > 30$ GeV and $|\eta| < 2.4$, a veto on b-quark jet tags, dijet separation $|\Delta\eta_{jj}| < 1.4$, and dijet

mass $70 < m_{jj} < 100$ GeV. False missing energy is reduced by requiring a minimum azimuthal separation $|\Delta\phi| < 0.4$ between the highest E_T jet and $E_{\mathrm{T}}^{\mathrm{miss}}$, and false photon backgrounds from Z bosons in the electron channel are reduced by vetoing electron-photon pairs consistent with the Z mass ($|M_Z - m_{e\gamma}| < 10$ GeV).

The photon E_T of selected events is shown in Fig. 13. The leading background is from $W\gamma$+jets production and is estimated from extrapolation of the m_{jj} sideband data into the signal region. Multijet background is extrapolated from a control sample with low $E_{\mathrm{T}}^{\mathrm{miss}}$, and the other backgrounds such as top quarks are estimated from simulation. 322 events are observed where 342 ± 16 were expected, of which 13 were expected to come from $WV\gamma$ production. An upper limit at 95% confidence level is obtained of 311 fb for the inclusive cross section, which is 3.4 times larger than the standard model prediction of `aMC@NLO` (91.6 ± 21.7 fb).

The binned photon E_T distribution in Fig. 13 is used to extract limits on dimension 6 EFT couplings a_0^W/Λ^2 and a_C^W/Λ^2, which affect $WW\gamma\gamma$ interactions, and κ_0^W/Λ^2 and κ_C^W/Λ^2, which affect $WWZ\gamma$ interactions. The magnitude of the limits are in the range of 12 TeV^{-2} to 34 TeV^{-2}. Limits on the dimension 8 EFT couplings $f_{T,0}/\Lambda^4$, $f_{M,0}/\Lambda^4$, $f_{M,1}/\Lambda^4$, $f_{M,2}/\Lambda^4$, and $f_{M,3}/\Lambda^4$ are also obtained, in the range of 25 TeV^{-4} for $f_{T,0}/\Lambda^4$ and $40 - 131$ TeV^{-4} for $f_{M,i}/\Lambda^4$.

4. Exclusive boson production

4.1. Exclusive single boson production, vector-boson fusion

By analysis of more exclusive selection of single or multiple electroweak boson production, it is possible with the LHC Run 1 data to isolate purely electroweak amplitudes of increased complexity and complementary sensitivity to new physics. The first demonstration of this was the observation of an electroweak amplitude in Z+2 jet production by both the ATLAS and CMS experiments [36, 37].

Figure 14 shows the leading order diagrams for Z+2 jet production from purely electroweak contributions. It includes a vector boson fusion component similar to VBF Higgs production, as well as electroweak bremsstrahlung amplitiudes. The different amplitudes are strongly interfering and cannot be practically isolated from one another via kinematic selection. In general, Z+2 jet production is dominated by simpler Drell-Yan production accompanied by QCD bremsstrahlung, but in certain exclusive regions of the dijet phase space the electroweak amplitudes are dominant.

The LHC experiments have used several criteria to isolate the electroweak amplitudes. The ATLAS analysis defines a search region with

- minimum p_{T} of the jets (45-55 GeV) and the Z boson candidate (20 GeV)
- minimum invariant mass of the dijet system (250 GeV)
- a veto on events with an additional jet in the rapidity gap between the leading two jets

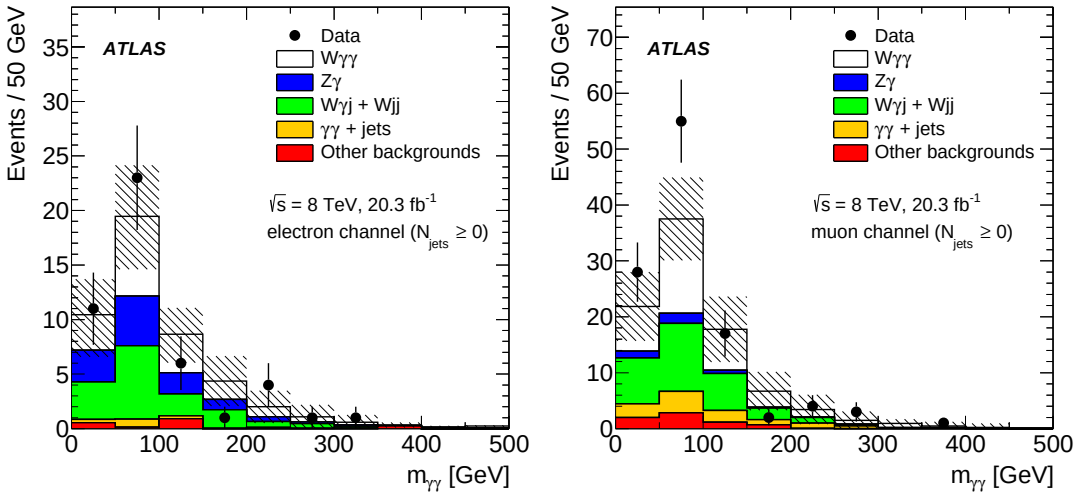

Figure 11. Diphoton invariant mass distribution of $W\gamma\gamma$ candidates selected by ATLAS [33]. Inclusive $e\nu\gamma\gamma$ (left) and $\mu\nu\gamma\gamma$ (right) candidates are shown separately.

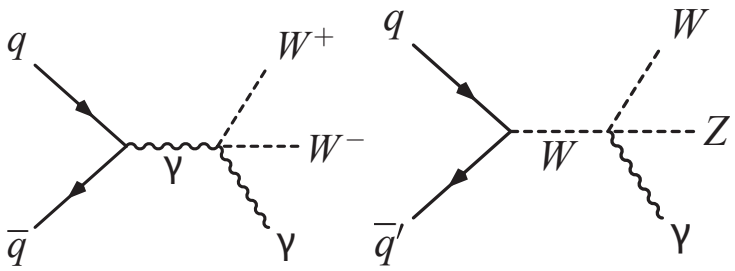

Figure 12. Quartic gauge boson interaction Feynman diagrams for $WW\gamma$ and $WZ\gamma$ production [35].

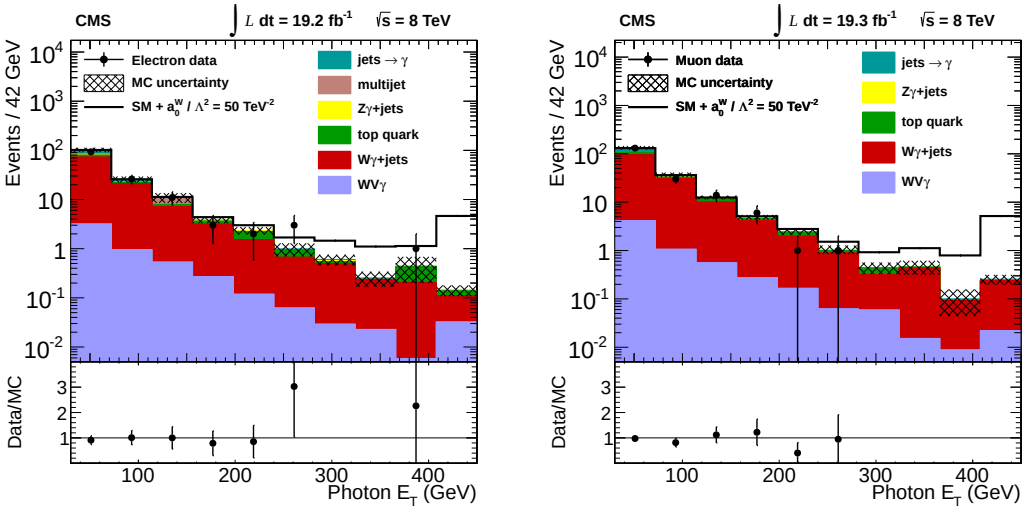

Figure 13. Photon E_{T} distribution of $WV\gamma$ candidates selected by CMS [35].

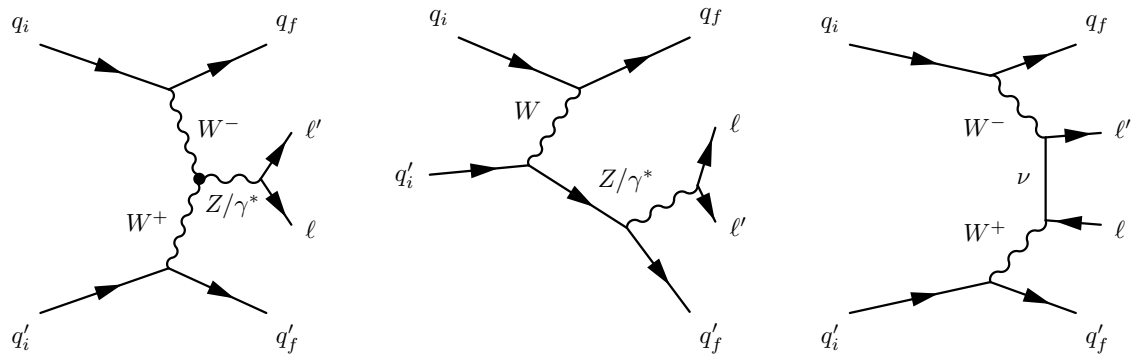

Figure 14. Representative Feynman diagrams for dilepton production in association with two jets from purely electroweak contributions: (left) vector boson fusion, (middle) bremsstrahlung-like, and (right) multiperipheral production.

- an upper limit (0.15) on the relative imbalance in the momenta of the four-body dilepton and dijet system, where imbalance is defined as the magnitude of the four-body p_{T} vector sum relative to the four-body scalar sum of transverse momenta.

CMS selects events with minimum p_{T} of the jets (30-50 GeV), minimum invariant mass of the dijet system (200 GeV), a maximum magnitude of the difference between the Z rapidity and the avarage jet rapidity (1.2), and an upper limit (0.14) on the relative imbalance of the three-body Z and dijet system. Additionally a multivariate discriminant is constructed which includes:

- the dijet invariant mass
- the sum of the magnitudes of the jet rapidities
- the Z boson rapidity
- the Z boson p_{T}
- ratio of the difference between the Z rapidity and the avarage jet rapidity to the dijet rapidity difference
- a quark/gluon multivariate discriminant evaluated for the leading two jets

The ATLAS analysis extracts an electroweak signal from selected events via a maximum likelihood fit of electroweak Z+2 jet signal and background yields to the dijet invariant mass distribution. The signal template is obtained from `Sherpa` Z+2 jet simulation and the background template also from `Sherpa`, except its shape is reweighted to obtain agreement with a separate control sample in the data. The result of the fit is shown in Figure 15. An excess of data over background begins to be seen near 1000 GeV in dijet mass, increasing in significance for higher dijet masses, totalling close to 1700 events with a statistical significance greater than 5σ. A high-purity fiducial cross section region is defined for events in the search region above 1000 GeV in dijet mass, where the signal yield is obtained from integrating the signal component of the likelihood fit. The resulting electroweak cross section is

$$\sigma_{EW}(m_{jj} > 1 \text{ TeV}) = 10.7 \pm 0.9(\text{stat}) \pm 1.9(\text{syst}) \pm 0.3(\text{lumi}) \text{ fb}$$

,

in agreement with the `Powheg` prediction of 9.4 ± 0.3 fb. The systematic uncertainty is predominantly from control sample statistics for background reweighting, the simulation modelling of signal and background, and estimates of the effect of neglecting signal-background interference.

Similarly, CMS extracts an electroweak signal via a likelihood fit to the kinematic multivariate discriminant. The signal and background templates are obtained from `MadGraph`, and an interference term is introduced proportional to the square root of the signal strength. The background shape is not reweighted but comparisons between data and simulation control samples bound shape uncertainties. A signal significance greater then 5σ is observed, corresponding to a signal yield close to 1600 events, as shown in Figure. 15. For a fiducial cross section corresponding to all selected events, they obtain

$$\sigma_{EW} = 174 \pm 15(\text{stat}) \pm 40(\text{syst}) \text{ fb}$$

,

in agreement with the `MadGraph` prediction of 208 ± 18 fb. Systematic uncertainties types and sizes are similar to that of ATLAS.

4.2. Exclusive di-boson production, vector-boson scattering

In addition to exclusive single boson production, CMS and ATLAS have evidence for exclusive diboson production, in two different channels. In one of them, CMS [38] has performed a search for exclusive diboson production via protons emitting (possibly quasi-) real photons which rescatter to produce W^+W^- pairs: $pp \rightarrow p^{(*)}W^+W^-p^{(*)} \rightarrow p^{(*)}\mu^\pm e^\mp p^{(*)}$, where p^* admits the possibility that the protons dissociate into an undetected system. Such production is characterized by a $\mu^\pm e^\mp$ pair which has no underlying event activity typical of proton-proton hard scattering. By selecting a $\mu^\pm e^\mp$ pair of sufficiently high individual (20 GeV) and joint (30 GeV) transverse momentum, and requiring further that the two lepton tracks intersect with each other, but have no additional tracks nearby, an exclusive production signal is isolated from backgrounds such as exclusive Drell-Yan and inclusive dilepton production from various hard scattering mechanisms, respectively. Selection efficiency is validated by examining a control sample of exclusive same-flavor Drell-Yan production ($p^{(*)}\mu^\pm\mu^\mp p^{(*)}$ or $p^{(*)}e^\pm e^\mp p^{(*)}$) and comparing it with simulated efficiency. The relative contribution of dissociated proton scattering for signal is also deduced by comparing the observed exclusive Drell-Yan cross section with an exclusive matrix element calculation (`LPAIR` [39, 40]); proton dissociation is estimated to enhance the signal by a factor of 4.10 ± 0.43 with respect to an exclusive calculation from `MadGraph`.

Figure 16 shows the distributions of dilepton p_{T} and extra tracks in data compared with expectations from simulation. 13 events are observed with an expected background

of 3.9 ± 0.6 in the 8 TeV data. In the 7 TeV [41] and 8 TeV data combined, a 3.4 σ excess is observed over background as evidence for exclusive (plus dissociative) W^+W^- production. The signal corresponds to a cross section in the 8 TeV data of $11.9^{+5.6}_{-4.5}$ fb, in agreement with a SM prediction of 6.9 ± 0.6 fb. Exclusive W^+W^- production is sensitive to $WW\gamma\gamma$ quartic couplings. The CMS analysis derived limits on the dimension 6 couplings a_0^W/Λ^2 and a_C^W/Λ^2 and, in the context of dimension 8 EFT, the anomalous couplings $f_{M(0,1,2,3)}/\Lambda^4$. The 95% CL upper limits are $1.1(4.4) \times 10^{-4}\text{GeV}^{-2}$ for a_0^W/Λ^2 (a_C^W/Λ^2), and range from $2 - 17 \times 10^{-4}\text{GeV}^{-4}$ for dimension 8 couplings, for models with no form factor. This process is the single best constraint on $WW\gamma\gamma$ QGCs.

The other exclusive diboson process for which the LHC has evidence is same-sign WW production, via the process $qq \to WW + 2q \to \ell^\pm\ell^\pm + 2\text{jet} + \text{E}_\text{T}^\text{miss}$. Similar to exclusive single boson production, the final state of interest is a superposition of several amplitudes at leading order, some of which are purely electroweak and include triple and quartic gauge boson interactions (see Fig. 17), and some of which have the final state jets arise from QCD initial- and final-state radiation. Through a suitable choice of final state phase space, the electroweak amplitudes are enhanced and the associated signal strength and distributions can be tested against the electroweak theory. The same-sign WW final state has the advantage over other exclusive diboson channels (W^+W^- or WZ) of a smaller relative QCD amplitude and smaller multi-lepton backgrounds from top quark, Drell-Yan, and WZ processes due to the same-sign dilepton requirement.

An ATLAS analysis [42] selects an "inclusive region" which is an admixture of electroweak and QCD contributions, and a VBS signal region which is predominantly electroweak. The inclusive region requires two same-sign leptons with $p_\text{T} > 25$ GeV, $E_\text{T}^\text{miss} > 40$ GeV, and at least two jets with $m_{jj} > 500$ GeV for the two highest p_T jets; the VBS region further requires that the two highest p_T jets are separated in rapidity, $|\Delta y_{jj}| > 2.4$. To reduce Drell-Yan background, events with dilepton mass less than 20 GeV or dielectrons within 10 GeV of the Z mass are vetoed. Top quark background is reduced by vetoing events with b-tagged jets. Finally, WZ background is reduced by vetoing events with a third lepton with muon $p_\text{T} > 6$ GeV or electron $p_\text{T} > 7$ GeV. This results in 50 events selected for the inclusive region (as shown in Fig. 18) and 34 for the VBS region. About half of selected events in either region are backgrounds from WZ, $W\gamma$ with photon conversion, and misidentified leptons from jets in V + jet processes. The significance of the signal in the inclusive region is observed (expected) to be 4.5σ (3.4σ), and for the VBS region the significance is observed (expected) to be 3.6σ (2.8σ). The measured cross sections in these two regions are $2.1 \pm 0.5(\text{stat}) \pm 0.3(\text{syst})$ fb and $1.3 \pm 0.4(\text{stat}) \pm 0.2(\text{syst})$ fb, comparing well with SM predictions from `Powheg-Box` [43, 44, 45, 46, 47, 48] of 1.52 ± 0.11 fb and 0.95 ± 0.06 fb, respectively.

The VBS cross section is used to constrain parameters of an effective chiral Lagrangian theory of vector boson scattering [49], calculated by `Whizard` [50, 51]: $0.14 < \alpha_4 < 0.16$ and $0.23 < \alpha_5 < 0.24$ limits are obtained at 95% CL.

A CMS analysis [52] selects events similar to the ATLAS VBS region: two same-

sign leptons with $p_{\mathrm{T}} > 20$ GeV, two jets with $m_{jj} > 500$ GeV and $|\Delta\eta_{jj}| > 2.5$, and $E_{\mathrm{T}}^{\mathrm{miss}} > 40$ GeV. There is a same-flavor Drell-Yan veto for events with dilepton mass less than 50 GeV or dielectrons within 15 GeV of the Z mass, a veto of top-like events with secondary vertex or soft muon tags, and a third lepton veto for $p_{\mathrm{T}} > 10$ GeV. The 12 events so selected are shown in Fig. 18. About half of them are expected to be background, mostly from misidentified leptons. The resulting excess has a significance of 1.9σ (2.9σ) observed (expected) for the purely electroweak amplitude. The observed fiducial cross section is $4.0^{+2.4}_{2.0}(\mathrm{stat})^{+1.1}_{1.0}(\mathrm{syst})$ fb compared to an expected cross section estimated from `VBFNLO` [53, 54, 55] of 5.8 ± 1.2 fb.

The $m_{\ell\ell}$ distribution of selected events is used to obtain 95% CL bounds on dimension 8 EFT couplings $f_{S,(0,1)}$, $f_{M,(0,1,6,7)}$, and $f_{T,(0,1,2)}$ [34]. For $f_{S,(0,1)}$, which can correspond to a spin-one VBS resonance, the limits are $-42\mathrm{TeV}^{-4} < \mathrm{f}_{\mathrm{S},0}/\Lambda^4 < 43\mathrm{TeV}^{-4}$ and $-129\mathrm{TeV}^{-4} < \mathrm{f}_{\mathrm{S},1}/\Lambda^4 < 131\mathrm{TeV}^{-4}$.

4.3. Z A_{FB} and $\sin^2\theta_W^{eff}$

In the electroweak theory the mixing angle θ_W is a free parameter indicating the degree of mixing between $SU(2)_L$ and $U(1)_Y$ neutral gauge bosons upon electroweak symmetry breaking to obtain the physical neutral gauge bosons γ and Z. Experimentally, it is typically measured as $\sin^2\theta_W$ via angular distributions in fermion pair production; it has been most precisely measured at the LEP 1 and SLD experiments via fermion pair production at the Z pole, yielding a combined value of 0.23153 ± 0.00016 [56]. In the Standard Model it is related to the gauge boson masses at tree level by $1 - m_W^2/m_Z^2$ and modified by higher-order loop corrections, including contributions from Higgs boson loops; the effective angle measured upon introducing loop corrections is denoted as $\sin^2\theta_W^{eff}$. The recent high-precision Higgs boson mass measurement at the LHC combined with other electroweak measurements can be used to predict a value for $\sin^2\theta_W^{eff}$ of 0.23149 ± 0.00007 [57], motivating an improvement upon the direct experimental measurement precision by a factor of two or more at the LHC to constrain the electroweak theory further.

At a hadron collider, fermion pair production at and around the Z pole is measured in the process $q\bar{q} \to \gamma^*/Z \to \ell^+\ell^-$, where the differential scattering cross section is characterized by $d^3\sigma/dm\,dy\,d\cos\theta = A(m,y)(1+\cos^2\theta) + B(m,y)\cos\theta$, where m is the final state lepton pair mass, y is the lepton pair rapidity, and $\cos\theta$ is the polar angle of the positive lepton with respect to the quark direction. A non-vanishing forward-backward asymmetry in this angle, $A_{FB}(m,y) = 3B(m,y)/8A(m,y)$, arises from interference between vector and axial-vector currents; the portion of $A_{FB}(m,y)$ corresponding to self-interference of the Z boson currents is directly sensitive to $\sin^2\theta_W^{eff}$.

In hadron collisions, the quark direction is ambiguous, as it may originate from either incoming hadron and have unknown transverse momentum. The impact of quark transverse momentum on the forward-backward assignment is minimized by defining the quark direction to be the difference between the forward-going and backward-going

hadron momentum vectors in the lepton pair rest frame, as originally suggested by Collins and Soper [58]; this angle is typically denoted as $\cos\theta^*$. In proton-proton collisions, the ambiguity due to quark origination is an irreducible dilution in A_{FB} which is strongest at low $|y|$ and decreasing at higher $|y|$ where valence quark/sea anti-quark annihilation is predominant; measurements of $A_{FB}(m, y)$ at high-$|y|$ are therefore intrinsically more sensitive to the undiluted value and have smaller theory uncertainties related to PDFs. In proton–anti-proton collisions, valence quark/valence anti-quark annihilation predominates, and so dilution and its associated uncertainties are vastly reduced, making the Tevatron experimental measurements [59, 60, 61] a competitive alternative to the LHC for current data samples. Three LHC experiments have measured $\sin^2\theta_W^{eff}$: an initial exploratory measurement by CMS at 7 TeV [62], a measurement by ATLAS with all 7 TeV data [63], and a measurement by LHCb [64, 65] with all 7 and 8 TeV data [66].

The ATLAS measurement was performed with three different samples: muon pairs with $P_T > 20$ GeV and $|\eta| < 2.4$; electron pairs with $E_T > 25$ GeV and $|\eta| < 2.47$; and electron pairs with $E_T > 25$ GeV where one has $|\eta| < 2.47$ and the other has $2.5 < |\eta| < 4.9$. In the last case the forward electron is identified with calorimetry alone, and the resulting pairs noentheless have a signal purity at the Z pole of 95%. The data in each sample i are binned in mass, and the raw measured angular asymmetry in that region of phase space, $A_{FB,i}^{\rm meas}(m)$, is computed from counting forward ($\cos\theta^* > 0$) and backward ($\cos\theta^* < 0$) candidates after background subtraction. Each $A_{FB,i}$ is used to extract $\sin^2\theta_W^{eff}$ via a binned χ^2 fit of LO `PYTHIA` templates of different mixing angle values to the data. Figure 19 shows the $\cos\theta^*$ distribution for selected central-forward electron pairs; an asymmetry between forward and backward angles is visually evident. Figure 19 also show the resulting $A_{FB}^{\rm meas}(m)$, alongside the best-fit predictions from LO `PYTHIA` and NLO `POWHEG`. The three samples give consistent values for $\sin^2\theta_W^{eff}$ and are combined to give a value of $0.2308 \pm 0.0005(\text{stat.}) \pm 0.0006(\text{syst.}) \pm 0.0009(\text{PDF})$, where the last term denotes the leading uncertainty in $\sin^2\theta_W^{eff}$ from uncertainties in specially prepared LO PDFs consistent with the LO PYTHIA template generation and 7 TeV ATLAS W and Z data (ATLAS-epWZ12 LO) [67]. A general feature of precision electroweak measurements at the LHC is the predominance of PDF uncertainties, requiring simultaneous PDF measurement with the parameter of interest to obtain the best precision. Other leading systematic uncertainties are the lepton energy scale and MC template statistics, which will improve with larger data sets.

The LHCb measurement employs a very similar technique. They select muon pairs with $P_T > 20$ GeV, $60 < m_{\mu\mu} < 160$ GeV, and $2.0 < |\eta| < 4.5$, with a signal mass resolution and purity similar to ATLAS but in a more forward, and therefore more sensitive, Z production region. LHCb operational instantaneous luminosity is limited to the range $2 - 4 \times 10^{32}\text{cm}^{-2}\text{s}^{-1}$, however, so the sample size is limited to 1fb^{-1} at 7 TeV and 2fb^{-1} at 8 TeV. The data are binned in mass and $A_{FB}(m)$ is computed for their acceptance, and then subsequently unfolded to account for mass resolution effects. Figure 20 shows the unfolded A_{FB} distribution at 8 TeV compared with NLO predictions

from POWHEG-BOX. The unfolded $A_{FB}(m)$ distribution is used to extract $\sin^2\theta_W^{eff}$ via a χ^2 fit of POWHEG-BOX templates of different mixing angle values to the data. They measure $\sin^2\theta_W^{eff} = 0.23142 \pm 0.00073(\text{stat.}) \pm 0.00052(\text{syst.}) \pm 0.00056(\text{th.})$, where the last term denotes uncertainties from theoretical modelling ingredients, predominantly PDFs. The PDF uncertainties are evaluated from QCD+QED NLO NNPDF 2.3 [68, 69], which, similar to the ATLAS PDF, includes 7 TeV electroweak production data from the LHC. In contrast to the ATLAS result, the LHCb measurement is statistics limited, but has 30% smaller theoretical uncertainties due to better understood PDF uncertainties in the more forward production region.

A comparison of experimental measurements of $\sin^2\theta_W^{eff}$ [59] is shown in Figure 21. The best single measurements from the Tevatron are more than twice as precise as the best measurements from the LHC, and the separate $A_{FB}^{0,b}$ and A_l results from e^+e^- collisions are more than four times as precise. There are reasonable prospects for the LHC experiments eventually surpassing these: ATLAS and CMS are expected to have superior statistical uncertainties by the end of Run 2, and all of the systematic and PDF uncertainties are expected to improve as well with larger electroweak data samples.

4.4. W boson mass

5. Summary

The ATLAS and CMS experiments at the LHC have published a first set of electroweak measurements with the run-1 data-sets at a collision energy of 7 TeVand 8 TeV, probing the electro-weak sector at the hitherto highest available scales. We started with the discussion of precision measurents of Drell-Yan production, a well understood electroweak process that in turn is used to validate theoretical calculations with higher order corrections in α_s and the PDF's of the proton. The total and differential cross section measurements help to reduce the theoretical cross section uncertainties of multi-boson processes, which are generally of the same order as the current experimental uncertainties. We reviewed the set of results available so far on inclusive di-boson production at the LHC. All inclusive di-boson final states ($W^+W^-, W^\pm Z, ZZ, W^\pm\gamma, Z\gamma$) have been observed and cross section measurements are available for collision energies of 7 TeV and 8 TeV. The complete set of measurements from both ATLAS and CMS including leptonic and semi-leptonic decay channels is expected to be published towards the end of 2016. A highlight of the electroweak physics program at the LHC is the observation of electroweak production channels that became accessible for the first time, namely processes with three vector bosons in the final state, and vector boson scattering processes that are characterised by two forward jets and two vector bosons in the final state.

For most total and fiducial cross section measurements with the full run-1 dataset the systematic uncertainties already limit the precision. The exception are processes with cross sections below a few fb, e.g. tri-boson producion. To probe the validity of the standard model at high partonic centre-of-mass energy, $\hat{s}$, the limits set in the

framework of anomalous gauge couplings are surpassing legacy measurements at LEP and the Tevatron, and are expected to further improve with increases $\sqrt{s}$ and integrated luminosity.

The set of run-1 results once completed will present a unique legacy of electroweak precision results at $\sqrt{s}$ values of 7 and 8 TeV. The run-2 analysis extend the energy range to $\sqrt{s} = 13$ TeV and provide even more precise limits on anomalous gauge couplings. Potentially, the combination of ATLAS and CMS results will allow more stringent constraints. Also the combination with Higgs measurements in the framework of EFT with shared anomalous coupling operators is being actively pursued and will allow a further reduction of the allowed parameter space. Precision measurements or first observations of more Tri-boson production and VBS processes will become possible with the full run-2 data set.

Acknowledgments

Acknowledgments go here.

[1] Chatrchyan S *et al.* 2012 *Physics Letters B* **716** 30 – 61 ISSN 0370-2693 URL http://www.sciencedirect.com/science/article/pii/S0370269312008581
[2] Aad G *et al.* 2012 *Physics Letters B* **716** 1 – 29 ISSN 0370-2693 URL http://www.sciencedirect.com/science/article/pii/S037026931200857X
[3] Aad G *et al.* (ATLAS Collaboration) 2013 *Phys.Lett.* **B725** 223–242 (*Preprint* 1305.4192)
[4] Melnikov K and Petriello F 2006 *Phys. Rev.* **D74** 114017 (*Preprint* hep-ph/0609070)
[5] Li Y and Petriello F 2012 *Phys. Rev.* **D86** 094034 (*Preprint* 1208.5967)
[6] Khachatryan V *et al.* (CMS Collaboration) 2015 *Eur.Phys.J.* **C75** 147 (*Preprint* 1412.1115)
[7] Aad G *et al.* (ATLAS) 2014 *Eur. Phys. J.* **C74** 3134 (*Preprint* 1407.2410)
[8] Khachatryan V *et al.* (CMS) 2015 *JHEP* **04** 025 (*Preprint* 1412.6302)
[9] Aad G *et al.* (ATLAS Collaboration) 2013 *JHEP* **1303** 128 (*Preprint* 1211.6096)
[10] Aad G *et al.* (ATLAS) 2016 *Phys. Rev. Lett.* **116** 101801 (*Preprint* 1512.05314)
[11] Chatrchyan S *et al.* (CMS Collaboration) 2013 *JHEP* **1301** 063 (*Preprint* 1211.4890)
[12] Khachatryan V *et al.* (CMS Collaboration) 2015 (*Preprint* 1503.05467)
[13] Khachatryan V *et al.* (CMS) 2015 *Phys. Lett.* **B740** 250–272 (*Preprint* 1406.0113)
[14] Herndon M 2015 Limits on anomalous triple and quartic gauge couplings URL https://twiki.cern.ch/twiki/bin/view/CMSPublic/PhysicsResultsSMPaTGC
[15] LEP Electroweak Gauge-Couplings Group 2002 A combination of preliminary results on gauge boson couplings measured by the lep experiments URL http://lepewwg.web.cern.ch/lepww/tgc/summer02
[16] Aad G *et al.* (ATLAS Collaboration) 2012 *Eur.Phys.J.* **C72** 2173 (*Preprint* 1208.1390)
[17] Aad G *et al.* (ATLAS) 2016 (*Preprint* 1603.02151)
[18] Aad G *et al.* (ATLAS Collaboration) 2013 *Phys.Rev.* **D87** 112001 (*Preprint* 1210.2979)
[19] Chatrchyan S *et al.* (CMS Collaboration) 2013 *Eur.Phys.J.* **C73** 2610 (*Preprint* 1306.1126)
[20] Chatrchyan S *et al.* (CMS Collaboration) 2013 *Phys.Lett.* **B721** 190–211 (*Preprint* 1301.4698)
[21] Gounaris G *et al.* 1996 Triple gauge boson couplings *AGS / RHIC Users Annual Meeting Upton, New York, June 15-16, 1995* (*Preprint* hep-ph/9601233) URL http://alice.cern.ch/format/showfull?sysnb=0215385
[22] Aad G *et al.* (ATLAS Collaboration) 2015 *JHEP* **1501** 049 (*Preprint* 1410.7238)
[23] Chatrchyan S *et al.* (CMS Collaboration) 2013 *Eur.Phys.J.* **C73** 2283 (*Preprint* 1210.7544)
[24] Hagiwara K, Ishihara S, Szalapski R and Zeppenfeld D 1992 *Physics Letters B* **283** 353 – 359 ISSN 0370-2693 URL http://www.sciencedirect.com/science/article/pii/037026939290031X

[25] Hagiwara K, Ishihara S, Szalapski R and Zeppenfeld D 1993 *Phys. Rev. D* **48**(5) 2182–2203 URL http://link.aps.org/doi/10.1103/PhysRevD.48.2182
[26] Chatrchyan S *et al.* (CMS Collaboration) 2014 *Eur.Phys.J.* **C74** 2973 (*Preprint* 1403.3047)
[27] Chatrchyan S *et al.* (CMS Collaboration) 2013 *JHEP* **1310** 164 (*Preprint* 1309.1117)
[28] Aad G *et al.* (ATLAS) 2016 *Phys. Rev. D* (*Preprint* 1604.05232)
[29] Aad G *et al.* (ATLAS Collaboration) 2013 *Phys.Rev.* **D87** 112003 (*Preprint* 1302.1283)
[30] Chatrchyan S *et al.* (CMS Collaboration) 2014 *Phys.Rev.* **D89** 092005 (*Preprint* 1308.6832)
[31] Khachatryan V *et al.* (CMS Collaboration) 2015 *JHEP* **1504** 164 (*Preprint* 1502.05664)
[32] Khachatryan V *et al.* (CMS) 2016 (*Preprint* 1602.07152)
[33] Aad G *et al.* (ATLAS Collaboration) 2015 (*Preprint* 1503.03243)
[34] Eboli O J P, Gonzalez-Garcia M C and Mizukoshi J K 2006 *Phys. Rev.* **D74** 073005 (*Preprint* hep-ph/0606118)
[35] Chatrchyan S *et al.* (CMS Collaboration) 2014 (*Preprint* 1404.4619)
[36] Aad G *et al.* (ATLAS Collaboration) 2014 *JHEP* **1404** 031 (*Preprint* 1401.7610)
[37] Khachatryan V *et al.* (CMS Collaboration) 2015 *Eur.Phys.J.* **C75** 66 (*Preprint* 1410.3153)
[38] Khachatryan V *et al.* (CMS) 2016 (*Preprint* 1604.04464)
[39] Vermaseren J A M 1983 *Nucl. Phys.* **B229** 347–371
[40] Baranov S P, Duenger O, Shooshtari H and Vermaseren J A M 1991 LPAIR: A generator for lepton pair production *In *Hamburg 1991, Proceedings, Physics at HERA, vol. 3* 1478-1482. (see HIGH ENERGY PHYSICS INDEX 30 (1992) No. 12988)*
[41] Chatrchyan S *et al.* (CMS Collaboration) 2013 *JHEP* **1307** 116 (*Preprint* 1305.5596)
[42] Aad G *et al.* (ATLAS Collaboration) 2014 *Phys.Rev.Lett.* **113** 141803 (*Preprint* 1405.6241)
[43] Nason P 2004 *JHEP* **11** 040 (*Preprint* hep-ph/0409146)
[44] Frixione S, Nason P and Oleari C 2007 *JHEP* **11** 070 (*Preprint* 0709.2092)
[45] Alioli S, Nason P, Oleari C and Re E 2010 *JHEP* **06** 043 (*Preprint* 1002.2581)
[46] Jager B, Oleari C and Zeppenfeld D 2009 *Phys. Rev.* **D80** 034022 (*Preprint* 0907.0580)
[47] Melia T, Melnikov K, Rontsch R and Zanderighi G 2010 *JHEP* **12** 053 (*Preprint* 1007.5313)
[48] Melia T, Nason P, Rontsch R and Zanderighi G 2011 *Eur. Phys. J.* **C71** 1670 (*Preprint* 1102.4846)
[49] Alboteanu A, Kilian W and Reuter J 2008 *JHEP* **11** 010 (*Preprint* 0806.4145)
[50] Kilian W, Ohl T and Reuter J 2011 *Eur. Phys. J.* **C71** 1742 (*Preprint* 0708.4233)
[51] Moretti M, Ohl T and Reuter J 2001 1981–2009 (*Preprint* hep-ph/0102195)
[52] Khachatryan V *et al.* (CMS Collaboration) 2015 *Phys.Rev.Lett.* **114** 051801 (*Preprint* 1410.6315)
[53] Baglio J *et al.* 2014 (*Preprint* 1404.3940)
[54] Arnold K *et al.* 2011 (*Preprint* 1107.4038)
[55] Arnold K *et al.* 2009 *Comput. Phys. Commun.* **180** 1661–1670 (*Preprint* 0811.4559)
[56] Schael S *et al.* (SLD Electroweak Group, DELPHI, ALEPH, SLD, SLD Heavy Flavour Group, OPAL, LEP Electroweak Working Group, L3) 2006 *Phys. Rept.* **427** 257–454 (*Preprint* hep-ex/0509008)
[57] Baak M, Cth J, Haller J, Hoecker A, Kogler R, Mnig K, Schott M and Stelzer J (Gfitter Group) 2014 *Eur. Phys. J.* **C74** 3046 (*Preprint* 1407.3792)
[58] Collins J C and Soper D E 1977 *Phys. Rev.* **D16** 2219
[59] Aaltonen T A *et al.* (CDF) 2016 (*Preprint* 1605.02719)
[60] Aaltonen T A *et al.* (CDF) 2014 *Phys. Rev.* **D89** 072005 (*Preprint* 1402.2239)
[61] Abazov V M *et al.* (D0) 2015 *Phys. Rev. Lett.* **115** 041801 (*Preprint* 1408.5016)
[62] Chatrchyan S *et al.* (CMS Collaboration) 2011 *Phys.Rev.* **D84** 112002 (*Preprint* 1110.2682)
[63] Aad G *et al.* (ATLAS Collaboration) 2015 (*Preprint* 1503.03709)
[64] Alves A Augusto J *et al.* (LHCb Collaboration) 2008 *JINST* **3** S08005
[65] Aaij R *et al.* (LHCb) 2015 *Int. J. Mod. Phys.* **A30** 1530022 (*Preprint* 1412.6352)
[66] Aaij R *et al.* (LHCb) 2015 *JHEP* **11** 190 (*Preprint* 1509.07645)
[67] Aad G *et al.* (ATLAS) 2012 *Phys. Rev.* **D85** 072004 (*Preprint* 1109.5141)
[68] Ball R D, Bertone V, Carrazza S, Del Debbio L, Forte S, Guffanti A, Hartland N P and Rojo J

(NNPDF) 2013 *Nucl. Phys.* **B877** 290–320 (*Preprint* 1308.0598)
[69] Ball R D *et al.* 2013 *Nucl. Phys.* **B867** 244–289 (*Preprint* 1207.1303)

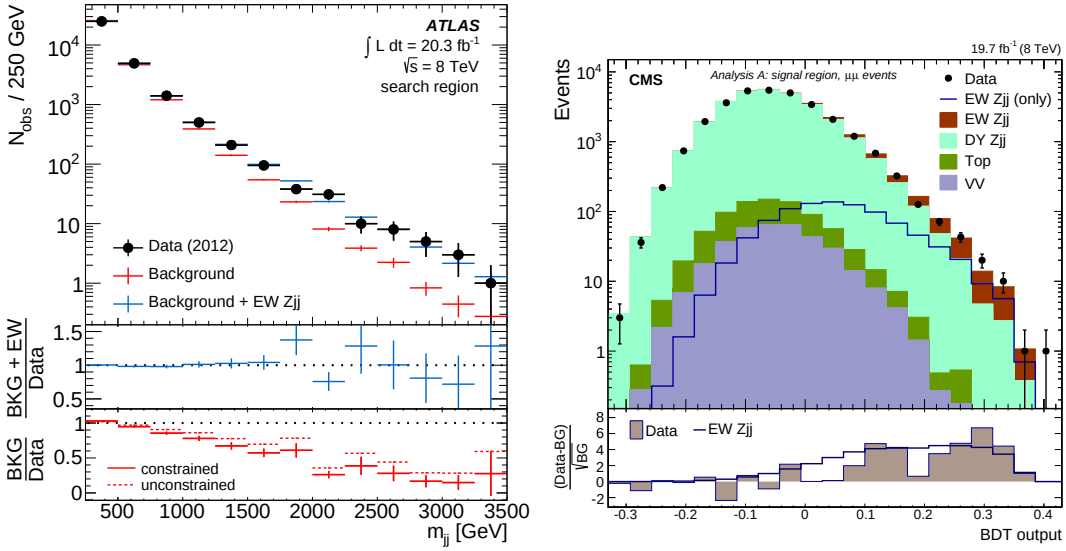

Figure 15. Evidence of observation of an electroweak amplitude in Z+2 jet production. Left: The invariant mass distribution of dijets in Z+2 jet events selected from a signal region by ATLAS. Right: The BDT distribution of Z+2 jet events selected from a signal region by CMS in the dimuon channel.

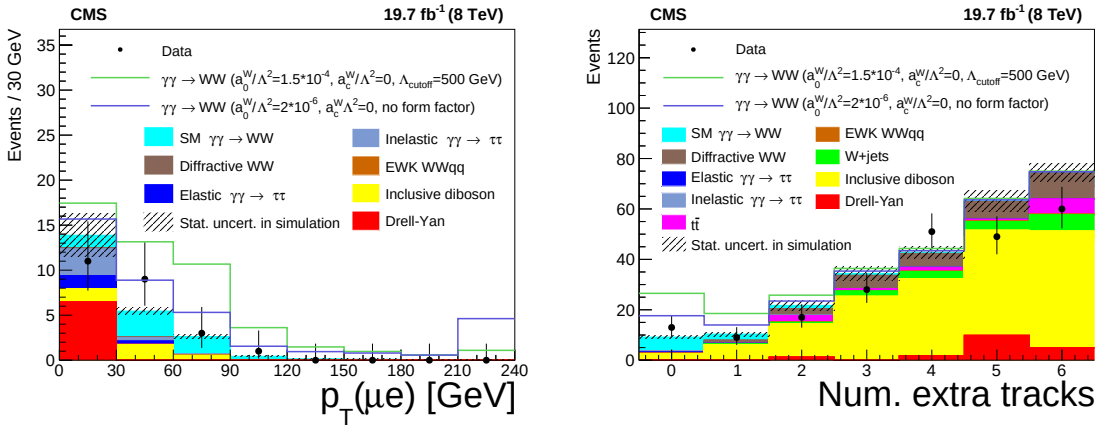

Figure 16. Evidence for exclusive diboson production via $pp \to p^{(*)}W^+W^-p^{(*)} \to p^{(*)}\mu^\pm e^\mp p^{(*)}$ [38]. Distributions of muon-electron transverse momentum for events with zero associated tracks (left), and extra-tracks multiplicity for events with $p_{\rm T}(\mu^\pm e^\mp) > 30$ GeV (right). The data are shown by the points with error bars; the histograms indicate the expected SM signal and backgrounds.

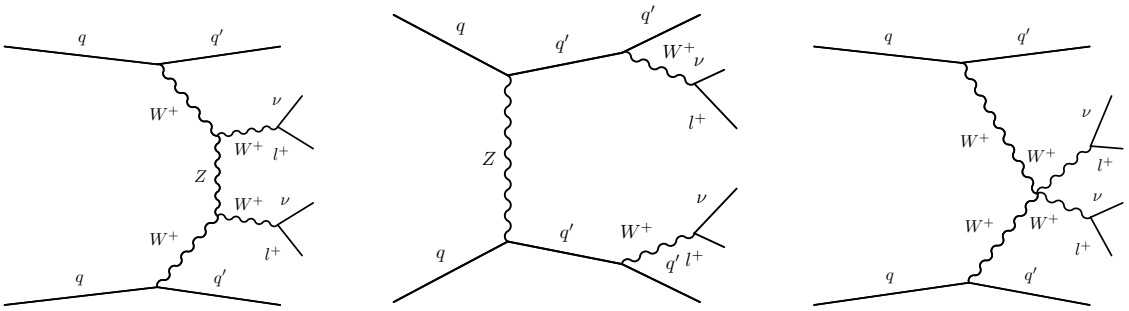

Figure 17. Representative Feynman diagrams for same-sign WW production in association with two jets from purely electroweak contributions: (left) vector boson fusion, (middle) bremsstrahlung-like, and (right) multiperipheral production [52].

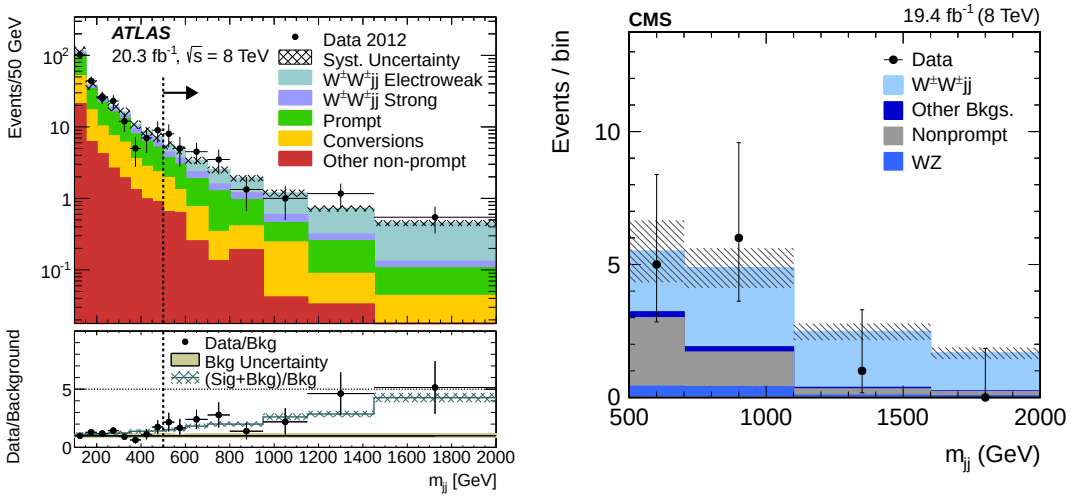

Figure 18. Left: Dijet invariant mass distribution of $W^{\pm}W^{\pm}jj$ candidates selected by ATLAS [42]. The inclusive signal region is indicated by the arrow. Right: Dijet invariant mass distribution of $W^{\pm}W^{\pm}jj$ candidates selected by CMS [52].

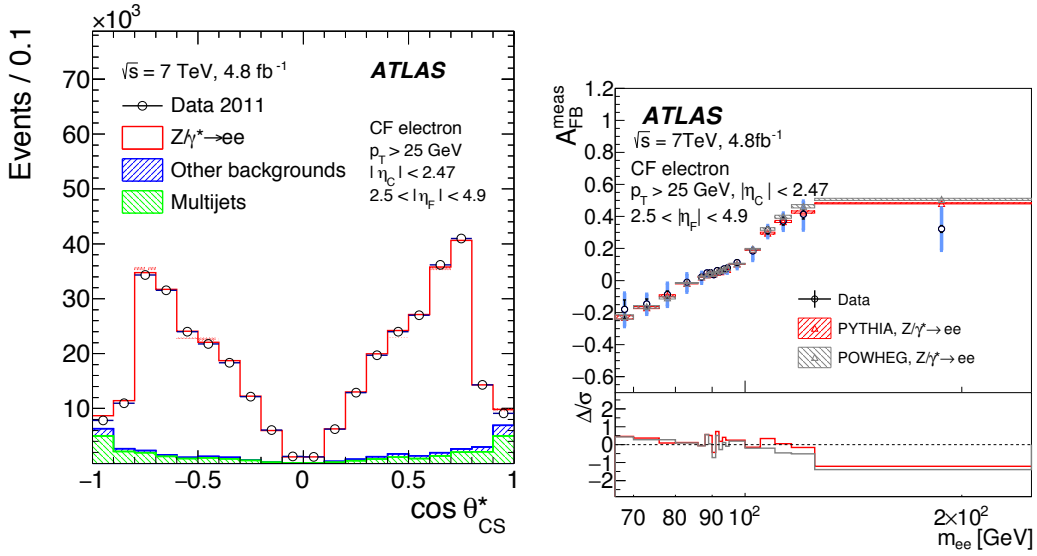

Figure 19. Left: The $\cos\theta^*$ distibution for selected central-forward electron pairs, compared with MC predictions. Right: $A_{FB}^{\mathrm{meas}}(m)$ for central-forward electron pairs, compared with MC predictions using the best fit $\sin^2\theta_W^{eff}$.

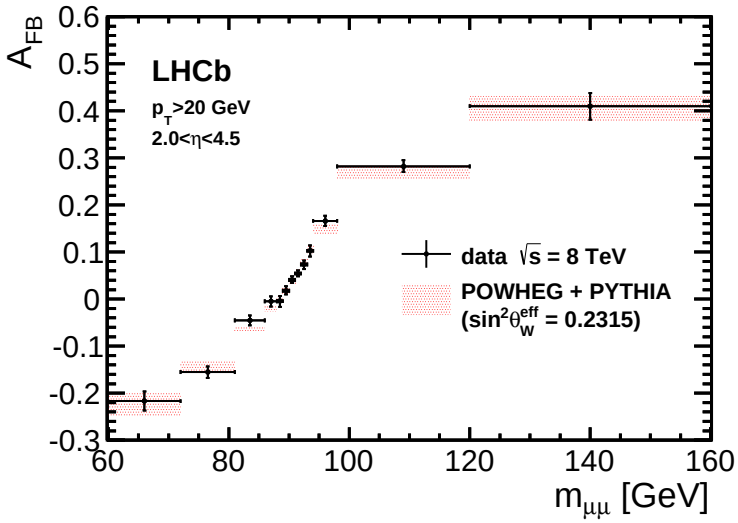

Figure 20. The unfolded A_{FB} distribution from LHCb 8 TeV data, as a function of dimuon mass, compared with NLO predictions from `POWHEG-BOX`.

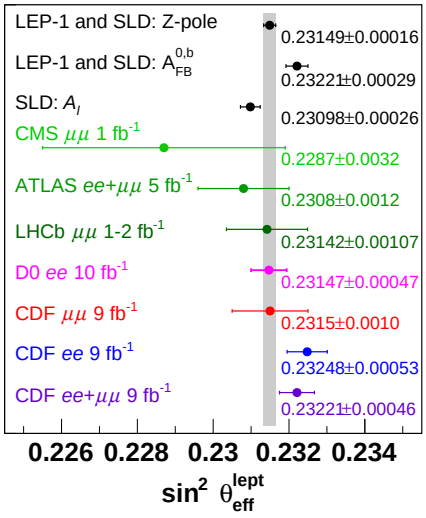

Figure 21. Comparison of experimental measurements of $\sin^2\theta_W^{eff}$ [59].